T follicular helper cell profiles differ by malaria antigen and for children compared to adults

Catherine S. Forconi[1], Christina Nixon[2], Hannah W. Wu[2], Boaz Odwar[3], Sunthorn Pond-Tor[2], John M. Ong'echa[3], Jonathan Kurtis[2], and Ann M. Moormann[1]*

[1]Division of Infectious Diseases and Immunology, Department of Medicine, University of Massachusetts Chan Medical School, Worcester, MA, USA

[2]Department of Pathology and Laboratory Medicine, Brown University, Providence, RI, USA

[3]Center for Global Health Research, Kenya Medical Research Institute, Kisumu, Kenya

*Corresponding author:

Ann Moormann, PhD, MPH, FAAS, FASTMH

Department of Medicine

Division of Infectious Diseases and Immunology

University of Massachusetts Chan Medical School

364 Plantation Street, LRB 313

Worcester, MA 01605 USA

Office: 508-856-8826 (VoIP)

Lab: 508-856-4562

Email: ann.moormann@umassmed.edu

Abstract

Background

Circulating T-follicular helper (cT_{FH}) cells have the potential to provide an additional correlate of protection against *Plasmodium falciparum* (*Pf)* as they are essential to promote B-cell production of long-lasting antibodies. Assessing the specificity of cT_{FH} subsets to individual malaria antigens is vital to understanding the variation observed in antibody responses and identifying promising malaria vaccine candidates.

Methods

Using spectral flow cytometry and unbiased clustering analysis, we assessed antigen-specific cT_{FH} cell recall responses *in vitro* to malaria vaccine candidates *Pf*-schizont egress antigen-1 (*Pf*SEA-1A) and *Pf*-glutamic acid-rich protein (*Pf*GARP) within a cross-section of children and adults living in a malaria-holoendemic region of western Kenya.

Findings

In children, a broad array of cT_{FH} subsets (defined by cytokine and transcription factor expression) were reactive to both malaria antigens, *Pf*SEA-1A and *Pf*GARP, while adults had a narrow profile centering on cT_{FH}17- and cT_{FH}1/17-like subsets following stimulation with *Pf*GARP only.

Interpretation

Because T_{FH}17 cells are involved in the maintenance of memory antibody responses within the context of parasitic infections, our results suggest that *Pf*GARP might generate longer-lived antibody responses compared to *Pf*SEA-1A. These findings have intriguing implications for evaluating malaria vaccine candidates as they highlight the importance of including cT_{FH} profiles when assessing interdependent correlates of protective immunity.

Keywords: T follicular helper, *Pf*-malaria, vaccine candidates, Kenya

Introduction

Despite progress made to reduce the global malaria burden, *Plasmodium falciparum* (*Pf*) remains one of the leading causes of mortality among children under 5 years of age.[1] Unfortunately, progress has been impeded by a plateau in malaria control since 2015. Anti-malarial drug resistance,[2,3] and unprecedented logistical challenges during the COVID-19 pandemic that dramatically impacted the distribution of insecticide-impregnated mosquito nets led to an increase in malaria cases in children under 5 years of age from 17.6 million in 2015 to 19.2 million in 2021 in East and Southern African countries,[1,4] thus, contributing to reinvigorated prioritization of malaria vaccine initiatives.

After 30 years of development, the first malaria vaccine—RTS,S/AS01E—was approved by the World Health Organization in 2021 for use in children residing in malaria-endemic regions. However, the limited efficacy of RTS,S,[5] particularly against severe malaria[5], has motivated the search for additional vaccine candidate antigens, including blood-stage *Pf*-schizont egress antigen-1 (*Pf*SEA-1A)[6] and *Pf*-glutamic acid-rich protein (*Pf*GARP).[7] Antibodies against *Pf*SEA-1A correlate with significantly lower parasite densities in Kenyan adults and adolescents and substantially reduce schizont replication *in vitro*.[6,8] Whereas *Pf*GARP-specific antibodies kill trophozoite-infected erythrocytes in culture and confer partial protection against *Pf*-challenge in vaccinated non-human primates.[7] The presence of antibodies against *Pf*GARP was associated with a 2-fold-lower parasite density in Kenyan adults and adolescents.[7] Due to the complexity of the parasites' life cycle, there is consensus that a multi-valent vaccine would be more efficacious[9]. However, determining which vaccine candidate antigens hold the most promise for inclusion in next-generation malaria vaccines remains a challenge.

Many pathogens and vaccines engender protective antibody responses after a single or few exposures[10], characterized by the production of long-lived plasma cells and memory B

cells.[11] Affinity maturation takes place in the germinal center (GC), where antigen-specific $CD4^{pos}$ T-follicular helper (T_{FH}) cells are required not only to provide cellular (CD40L) and molecular (IL-21, IL-4, and IL-13) signals to trigger B-cell proliferation but also to promote GC maintenance and plasmablast differentiation. The GC is also where higher affinity B cells outcompete B cells with lower affinity for T_{FH} help.[12,13] T_{FH} cells are defined by the expression of a combination of markers, starting with chemokine receptor CXCR5, which directs $CD4^{pos}$ T cells from the T-cell zone to engage with follicular B cells.[14,15] Once antigen-experienced T_{FH} cells leave the GC, they become circulating T_{FH} (cT_{FH}) cells and correlate with the generation of long-lasting antibody responses. Interestingly, cT_{FH} cells can also come from peripheral cT_{FH} precursor $CCR7^{low}PD1^{high}CXCR5^{pos}$ cells; thus, they also have a GC-independent origin[16]. Expression profiles of CCR6 and CXCR3 categorize cT_{FH} subsets as follows: $cT_{FH}1$ ($CCR6^{neg}CXCR3^{pos}$), $cT_{FH}2$ ($CCR6^{neg}CXCR3^{neg}$), and $cT_{FH}17$ ($CCR6^{pos}CXCR3^{neg}$)[17], whereas the expression of PD-1, ICOS, CD127, and CCR7 define their functional status: quiescent/central memory cT_{FH} ($CCR7^{high}PD\text{-}1^{neg}ICOS^{neg}CD127^{pos}$) or activated/effector memory cT_{FH} ($CCR7^{low}PD\text{-}1^{pos}ICOS^{pos}CD127^{low/neg}$).[17–19] In addition, transcription factors (i.e., Bcl6 and cMAF) and cytokines (i.e., interferon-gamma [IFN□], IL-4, and IL-21) are crucial to further characterizing the role of each cT_{FH} subset within the context of their interactions with B cells to promote antibody production.[20–23] Bcl6 facilitates the production of IL-21 by T cells which aids B-cell affinity maturation and antibody production.[24–26] T_{FH} cells also secrete cytokines that align with their subset classifications (but are not limited to them), such as IFN□ ($T_{FH}1$), IL-4/IL-13 ($T_{FH}2$), IL-4/IL-5/IL-13 ($T_{FH}13$), and IL-17 ($T_{FH}17$), that direct antibody isotype class-switching and mediate effector functions.[12,18,20–22,27]

Several studies have characterized cT_{FH} subsets within the context of both adult and childhood *Pf*-malaria infections, as well as in healthy malaria-naïve volunteers under

controlled malaria infection conditions.[28] In Mali, where malaria is seasonal, Obeng-Adjei and colleagues showed that T_H1-polarized cT_{FH} $PD1^{pos}CXCR5^{pos}CXCR3^{pos}$ cells were preferentially activated in children and less efficient than $CXCR3^{neg}$ cT_{FH} cells in helping autologous B cells produce antibodies; yet they used U.S. healthy adult cT_{FH} cells for their *in vitro* assays. Therefore, the authors suggested that promoting T_H2-like $CXCR3^{neg}$ cT_{FH} subsets could improve antimalarial vaccine efficacy.[29] Similarly, a recent study in Papua, Indonesia, where malaria is perennial, found that all cT_{FH} subsets from adults showed higher activation and proliferation compared to cT_{FH} cells from children.[30] After *in vitro* stimulation with infected red blood cells, they found that all cT_{FH} subsets were activated in adults accompanied by IL-4 production, whereas only the T_H1-polarized cT_{FH} subset responded in children.[30] One study in Uganda, where malaria is holoendemic with seasonal peaks, showed that a shift from T_H2- to T_H1-polarized cT_{FH} subsets occurred during the first 6 years of life and was associated with the development of functional antibodies against *Pf*-malaria, yet appeared to be independent of malaria exposure as this age-associated shift was also observed in a malaria-naïve population.[31] Interestingly, this study also found that a higher proportion of T_H17-cT_{FH} cells was associated with a decreased risk of *P. falciparum* infection the following year; however, the authors postulated that this phenomenon could have been driven by previous exposure to the parasite. The observed higher abundance of T_H2-like cT_{FH} cells in children younger than 6 years old and the age-associated increase in T_H1-cT_{FH} cells achieving the same proportion of T_H1-cT_{FH} cells by 6 years of age and into adulthood appeared to be independent of malaria exposure. Of note, these studies were limited by the use of a 2-dimensional gating strategy to classify cT_{FH} subsets and whole parasite activation conditions, either during infections or *in vitro* stimulation assays, leaving the malaria-antigen specificity of the different cT_{FH} subsets responses undefined. However, these studies highlight the progression in the field of evaluating the role of human T_{FH} cells in anti-malarial immunity.

Antibody levels are an unreliable predictor of malaria vaccine efficacy.[32] Thus, establishing a combined immune profile to incorporate other surrogates of protection is warranted. Here, we examined the profile of cT_{FH} subsets using multiparameter spectral flow cytometry[33,34] against two malaria vaccine candidate antigens (*Pf*SEA-1A[6] and *Pf*GARP[7]) in a cross-section of children and adults residing in a malaria-holoendemic region of Kenya. Our findings revealed significant differences in cT_{FH} subsets between children and adults, where children had more abundant $cT_{FH}1$-like cells and showed antigen-specific responses from all cT_{FH} types, whereas these responses were limited to $cT_{FH}17$- and 1/17-like cells in adults. Moreover, this study showed that *Pf*GARP triggered Bcl6 expression across cT_{FH} subsets, whereas *Pf*SEA-1A induced more cMAF expression, demonstrating the feasibility of implementing T-cell immune correlates to down-select new malaria candidates.

Results

Children had lower anti-PfSEA-1A antibodies compared to adults but similar levels of anti-PfGARP antibodies

This cross-sectional study selected a convenience sample of 7-year-old children and adults with a mean age of 22.67 years (ranging from 19 to 30 years old). No statistical difference was observed (p=0.35 after Welch's test) regarding the absolute lymphocyte count (ALC) between children (mean of 373.1; standard deviation [SD] of 118.1) and adults (mean of 335.2; SD of 99.08). Children had significantly lower hematocrit values (median of 37%, interquartile range [IQR] of 32.7–40.5) compared to adults (median of 44.4%, IQR of 40.5–46), p=0.002 after a two-tailed Mann-Whitney t-test; however, these values were within normal ranges after adjusting for age.[35] Both males and females (sex assigned at birth) were enrolled, with 43% (6/14) and 53% (8/15) being female within the children and adult groups, respectively. Seroprofiles against a panel of commonly used malaria antigens were generated

to confirm the history of previous malaria infections for the selected children (Figure 1a). All participants had high IgG levels against merozoite antigens, apical membrane antigen 1 (AMA-1) and merozoite surface protein (MSP1), confirming at least one malaria infection within their lifetime.[36,37] IgG antibodies against circumsporozoite protein (CSP) and CelTOS (liver-stage antigens) were characteristically lower than against blood-stage antigens yet were present in all study children. We observed a clear bimodal distribution in antibody levels against histidine-rich protein 2 (HRP2) with half of the children having "high-HRP2" versus "low-HRP2" IgG levels, possibly a reflection of recent malaria history since it has been suggested that HRP2-specific antibodies are short-lived and could serve as a surrogate for a recent infection.[38] We assessed serological profiles for two *Pf*-malaria antigens being considered as potential vaccine candidates,[6,7] *Pf*SEA-1A and *Pf*GARP (Figure 1b). We found that children had a significantly lower median level of IgG against *Pf*SEA-1A compared to adults ($p<0.0001$), whereas median levels to *Pf*GARP were similarly high for adults and children, yet with a broad range of reactivity.

The overall abundance of $CD4^{pos}CXCR5^{pos}$ cells is unaltered by in vitro antigen stimulation

To determine whether *in vitro* antigen stimulation with *Pf*SEA-1A or *Pf*GARP altered the abundance of total cT_{FH} cells, we compared cT_{FH} cells from adults and children using a FlowSOM unbiased clustering analysis and EMBEDSOM dimensional reduction based on common lineage markers assessed by spectral flow cytometry from 87,812 live lymphocytes from each sample: $CD8^{pos}$, $CD4^{pos}$, $CD4^{pos}CXCR5^{pos}$, and $CD4^{pos}CD25^{pos}$ (Figure 2a). As expected, after a short stimulation (6 hrs), overall abundances of cT_{FH} cells were similar across conditions for both adults (Figure 2b) and children (Figure 2c). This observation was confirmed by EdgeR statistical analysis (Supplemental Figure 2) and demonstrated that *in*

vitro stimulation did not preferentially expand the T cell populations on which we based our subsequent analyses.

An unbiased clustering analysis identifies twelve distinct cT_{FH} meta-clusters

Numerous markers and a two-dimensional gating strategy have previously been used to determine the frequency of cT_{FH} subsets.[29–31] To simultaneously account for the expression of 17 markers required to define cT_{FH} subsets, we used FlowSOM unbiased clustering analysis to determine the frequency of cT_{FH} subsets from a pool of 1,000 $CD3^{pos}CD4^{pos}CXCR5^{pos}CD25^{neg}$ cells from each sample (total of 13,000 $CD3^{pos}CD4^{pos}CXCR5^{pos}CD25^{neg}$ cells in both children and adults). Based on CXCR3 and CCR6 expression as well as the expression of effector/memory/activation markers (CCR7, CD127, PD1, and ICOS), cytokines (IFN□, IL-4, and IL-21), and transcription factors (Bcl6 and cMAF), we initially identified 15 meta-clusters within the $CD4^{pos}CXCR5^{pos}$ T cells (Figure 3a). First, we found different CXCR5 expression levels between meta-clusters (Figure 3b); CXCR5 is essential for cT_{FH} cells to migrate to the lymph nodes and interact with B-cells. Data presented in Figure 3 are from children; however, we found similar observations in the adult group (Supplemental Figure 3). Because $CD45RA^{pos}CXCR5^{pos}$ cells are likely naïve cells with transient low expression of CXCR5 yet high expression of CD45RA, we excluded 3 meta-clusters using these criteria (i.e., MC12, MC14, and MC15) (Figure 3c). Then, using the overall expression of CXCR3 and CCR6 across the cT_{FH} subsets (Figure 3d and 3e), we identified the remaining 12 clusters as follows: MC01 and MC02 were $cT_{FH}2$-like; MC06 and MC07 were $cT_{FH}1$-like; MC09 and MC11 were $cT_{FH}1/17$-like; MC10 and MC13 were $cT_{FH}17$-like. However, CXCR3 expression was not clearly delineated for some subsets and did not align with the conventional CCR6 vs. CXCR3 cytoplot (Figure 3f and 3g, Supplemental Figure 4). Based on the heatmap (Figure 3f), MC03, MC04, MC05,

and MC08 clusters appear closer to $cT_{FH}2$-like MC01 and MC02 clusters than $cT_{FH}1$-like clusters MC06 and MC07, suggesting that they might be part of the $cT_{FH}2$-like subset. But, based on their intensity of CXCR3 expression and their distribution across the CCR6 vs. CXCR3 cytoplot (Supplemental Figure 4), we defined MC03, MC04, MC05, and MC08 clusters as "undetermined" and would require additional cytokine and transcription factor analyses to fully categorize them.

Heterogeneity of activation/maturation markers within cT_{FH} subsets

By assessing the expression of CCR7, PD1, CD127, and ICOS (Figure 4) and following the three-dimensional expression patterns adapted from Schmitt et al.[17] (Supplemental Figure 5), we determined the activation state of each cT_{FH} meta-cluster and which markers created novel subsets. Data in Figure 4 are from children; however, similar observations were made for adults (Supplemental Figure 6). As expected, none of the extracellular markers showed significant differences in expression patterns after a short 6-hour stimulation, thus, representing the cT_{FH} repertoire present within our study participants. Interestingly, the $cT_{FH}1or2$ subset (MC03) was the only meta-cluster with high expression of PD1 (Figure 4a) accompanied by high ICOS (Figure 4b), low CCR7 (Figure 4c), and low CD127 expression (Figure 4d), suggesting that MC03 was an activated/effector $cT_{FH}1or2$ subset. The MC04 subset had low CCR7 and high ICOS expression but low CD127 and intermediate PD1 expression, indicating that this cluster was a less activated/effector $cT_{FH}1or2$ cluster compared to MC03.

We also observed additional nuances in the expression pattern for other $cT_{FH}1$-like meta-clusters. The $cT_{FH}1$-like MC06 cluster had an activated/effector profile, whereas the $cT_{FH}1$-like MC07 cluster had a quiescent/effector profile. The $cT_{FH}1or2$-like MC05 and

MC08 clusters were defined as quiescent/memory (overall high CCR7 expression) yet with very low expression of ICOS for the MC05 cluster.

Likewise, $cT_{FH}2$-like and $cT_{FH}17$-like meta-clusters also displayed heterogeneity. The $cT_{FH}2$-like MC01 cluster had an activated/effector profile, whereas the $cT_{FH}2$-like MC02 cluster seemed to be a quiescent/effector subset. The $cT_{FH}1/17$-like subsets MC09 and MC11 overall had an activated profile, although they had higher expression of CCR7 and CD127 compared to other subsets, suggesting an activated/memory phenotype. Finally, the $cT_{FH}17$-like MC10 cluster seemed quiescent, whereas $cT_{FH}17$-like MC13 had an activated/effector profile. Of note, because of our short stimulation time (6 hrs), we were unable to find statistical differences in the CD40L expression between groups as only few individuals responded through it (Supplemental Figure 7). However, our analysis methods revealed a higher degree of previously unrecognized heterogeneity within circulating cT_{FH} cells.

Activated $cT_{FH}1or2$-, $cT_{FH}1$-, and quiescent $cT_{FH}1or2$-like subsets were more abundant in children

After having deconvoluted cT_{FH} cells into 12 subsets, we next wanted to determine whether their abundance differed by age or after antigen stimulation. Using Uniform Manifold Approximation and Projection (UMAP) visualization, we found that cT_{FH} dimensional reduction was contiguous as meta-clusters merged with each other; in addition, there were notable differences between adults and children (Figure 5a). We found that activated $PD1^{high}$ $cT_{FH}1or2$-like (MC03), activated $cT_{FH}1$-like (MC06), and quiescent $ICOS^{high}$ $cT_{FH}1or2$-like (MC08) subsets were significantly more abundant in children compared to adults regardless of the stimulation conditions (Figure 5b, 5c, and 5d, $p<0.05$). In contrast, the quiescent *Pf*SEA-1A- and *Pf*GARP-specific $cT_{FH}2$-like cluster (MC02) was significantly more abundant in adults compared to children (Figure 5c and 5d, $p<0.05$). Interestingly, following

*Pf*GARP stimulation, the activated $cT_{FH}1/17$-like subset (MC09) became more abundant in children compared to adults (Figure 5d, $p<0.05$ with a False Discovery Rate=0.08), but no additional subsets shifted phenotype after *Pf*SEA-1A stimulation (Figure 5c). Of note, the activated $PD1^{low}$ $cT_{FH}1or2$-like cells (MC04) seemed more abundant in non-stimulated adults and *Pf*GARP-stimulated children, but, because these observations were not present in all the participants, they did not achieve statistical significance in EdgeR.

The abundance heatmap (Figure 5e) reiterates the differences observed between children and adults and highlights important considerations when assessing the potential role of each cT_{FH} subset in assisting with cognate antibody production. Overall, the most common cT_{FH} subset in both children and adults is the quiescent $cT_{FH}2$-like cells (MC02, 24.1% and 41.2% respectively). However, the antigen-specific differences in the cT_{FH} subset abundance for children (MC09 for *Pf*GARP) and for adults (MC02 for both *Pf*SEA-1A and *Pf*GARP) suggest that children engage different cT_{FH} cells as they are developing immunity. Of note, only the activated $PD1^{low}$ $cT_{FH}1or2$-like cells (MC04) was less abundant in children with low compared to high HRP2 antibody levels (Supplemental Figure 8), suggesting that this subset may be involved in short-term antibody production. Overall, this comprehensive examination of the abundance of cT_{FH} subsets demonstrates important diversity based on age and malaria-antigen specificity.

PfSEA-1A and PfGARP induced IL-4, Bcl6, and cMAF from a broad range of cT_{FH} subsets in children

Because the children in this cohort were 7 years of age and resided in a malaria-holoendemic area, they had ample time to develop premunition. To assess antigen-specific cytokine and transcription factor expression signatures and further characterize cT_{FH} subsets, we generated clustered heatmaps of the median fluorescence intensity (MFI) of each analyte (IFN□, IL-4,

IL-21, Bcl6, and cMAF) for children (Supplemental Figure 9a) and adults (Supplemental Figure 9b). Next, using these MFI data, we performed Wilcoxon paired two-tailed t-tests to compare *Pf*SEA-1A and *Pf*GARP stimulation to unstimulated cells (Figure 6a and 6b, respectively). Significant differences in these expression profiles allowed us to further characterize meta-clusters into three main groups. Group 1: cT_{FH}2-like (activated MC01 and quiescent MC02) and activated cT_{FH}1or2-like ($PD1^{high}$MC03 and $PD1^{low}$MC04); Group 2: activated and quiescent cT_{FH}1-like (MC06 and MC07); Group 3: activated cT_{FH}1/17-like (MC11) and cT_{FH}17-like (quiescent MC10 and activated MC13). For children, *Pf*SEA-1A and *Pf*GARP induced robust IL-4 expression in 9 out of 12 cT_{FH} meta-clusters (p-values ≤ 0.0105); although the composition of which cT_{FH} subsets were engaged differed slightly by antigen (quiescent cT_{FH}1or2-like $ICOS^{low}$ MC05 versus quiescent cT_{FH}2-like MC02, respectively). In contrast to IL-4, we observed no change in expression for IFN□ or IL-21 after *in vitro* antigen stimulation (except for quiescent cT_{FH}1or2-like $ICOS^{high}$ MC08, p-value=0.0391), suggesting that these cytokines are not informative to define the development of antigen-specific cT_{FH} subsets in children.

We found that *Pf*SEA-1A (Figure 6a) and *Pf*GARP (Figure 6b) induced similar Bcl6 and cMAF expression profiles from some of the same cT_{FH} subsets: both transcription factors were expressed by activated cT_{FH}2-like MC01 and quiescent cT_{FH}17-like MC10, but only cMAF was expressed in activated and quiescent cT_{FH}1-like MC06, MC07, and activated cT_{FH}1/17-like MC11 subsets. However, *Pf*SEA-1A induced Bcl6 and cMAF from activated $PD1^{high}$MC03, whereas *Pf*GARP only induced Bcl6. In contrast, the quiescent cT_{FH}2-like MC02 subset did not seem to respond to *Pf*SEA-1A (only cMAF was significant, p=0.0266, Figure 6a, Supplemental Figures 10 and 11), whereas *Pf*GARP stimulation induced significantly more IL-4, Bcl6, and cMAF compared to unstimulated cells (p=0.0081,

p=0.0017, and *p*=0.0081, respectively, Figure 6b, Supplemental Figures 10 and 11). We then compared the response intensity between *Pf*SEA-1A and *Pf*GARP stimulations and found significant differences in IFN□, IL-21, Bcl6, and cMAF expression levels (Figure 6c, 6d, 6e, and 6f, respectively). In Group 1, Bcl6 expression was significantly higher within activated and quiescent cT_{FH}2-like subsets (MC01 and MC02) as well as activated $PD1^{high}$ cT_{FH}1or2-like (MC03) cells after *Pf*GARP compared to *Pf*SEA-1A stimulation (*p*=0.0266, *p*=0.0134 and *p*=0.0327, respectively, Figure 6e). Within Group 2, IFN□ and Bcl6 were highly expressed by activated cT_{FH}1-like (MC06) after *Pf*GARP stimulation compared to *Pf*SEA-1A stimulation (*p*=0.0093 and *p*=0.0024, respectively, Figure 6c and 6e). Finally, within Group 3, the activated cT_{FH}1/17-like cells (MC11) expressed higher cMAF after *Pf*SEA-1A stimulation compared to *Pf*GARP (p=0.0186, Figure 6f). Interestingly, *Pf*GARP induced significantly more IL-21 within the quiescent $ICOS^{low}$ cT_{FH}1or2-like (MC05) meta-cluster compared to *Pf*SEA-1A stimulation (*p*=0.0186, Figure 6d). Non-significant differences in cytokines and transcription factors expressed by cT_{FH} subsets between conditions are shown in Supplemental Figures 12 and 13, respectively.

PfGARP induced IL-4, Bcl6, and cMAF expression in activated cT_{FH}1/17- and cT_{FH}17-like subsets in adults

A similar heatmap was generated for adult expression profiles comparing *Pf*SEA-1A and *Pf*GARP stimulated to unstimulated cells (Figure 7). Here, we found that both *Pf*SEA-1A and *Pf*GARP induced significant expression of both IFN□ and IL-4 for activated (MC01) and quiescent (MC02) cT_{FH}2-like cells (Figure 7a and 7b, Supplemental Figure 12). Whereas *Pf*GARP also induced IL-4 and IFN□ expression from quiescent and activated cT_{FH}17-like cells (MC10 and MC13), in addition to Bcl6 and cMAF for MC13 (Figure 7b, Supplemental Figure 13). This observation was surprising because IFN□ expression is commonly used to

categorize the $cT_{FH}1$ subset (Group 2); however, as shown earlier, quiescent and activated $cT_{FH}17$-like cells (MC10 and MC13) did not express CXCR3 (Figure 3d and 3e). In contrast, activated the $cT_{FH}1/17$-like cells (MC11) only responded to *Pf*GARP (Figure 7b, Supplemental Figure 12), expressing higher levels of IL-4, IL-21, Bcl6, and cMAF. Finally, while assessing the differences between the two malaria antigens, we found that *Pf*GARP induced more Bcl6 expression than *Pf*SEA-1A within the quiescent $cT_{FH}2$-like subset (MC02, p=0.0327) and the quiescent $ICOS^{low}$ $cT_{FH}1or2$-like cells (MC05, p=0.0105), as well as within the quiescent $cT_{FH}17$-like subset (MC10, p=0.0479) and the activated $cT_{FH}1/17$-like cells (MC11, p=0.0020) (Figure 7d). The MC11 cells also expressed higher IL-21 levels after *Pf*GARP compared to *Pf*SEA-1A stimulation (p=0.0273, Figure 7c); whereas *Pf*SEA-1A induced cMAF within the activated $cT_{FH}2$-like subset (MC01, p=0.0134) but *Pf*GARP did not (Figure 7e). Overall, the main observation for adults is that *Pf*SEA-1A predominantly induced IL-4 from slightly more than half of the cT_{FH} clusters, whereas *Pf*GARP induced a broader range of cytokines and transcription factors but within the activated $cT_{FH}1/17$-like cells (MC11) and quiescent and activated $cT_{FH}17$-like subset (MC10 and MC13) similar to children. This analysis shows clear differences in cT_{FH} subset specificity by malaria antigen and cT_{FH} subset engagement by age group, with the cT_{FH} repertoire becoming more restricted in adults compared to children.

The activated $cT_{FH}1or2$-like subset is more abundant in participants with high anti-PfGARP antibodies

As shown in Figure 1b, a broad range of anti-*Pf*GARP IgG antibody levels were found in both children and adults. Thus, we wanted to determine whether the abundance of any of the cT_{FH} subsets was associated with the level of anti-*Pf*GARP IgG antibodies. When stratifying by high versus low anti-*Pf*GARP IgG antibody levels, we found that an activated $cT_{FH}1or2$-

like subset (MC04) was more abundant in participants with high levels of anti-*Pf*GARP IgG for both children (Figure 8a) and adults (Figure 8b) after *Pf*GARP stimulation compared to participants with low levels or an absence of anti-*Pf*GARP IgG. However, even though the *p*-values were significant for both children and adults (p=0.02 and p=0.004, respectively), the FDR was less than 0.05 only for the adults (FDR=0.018). This suggests that this particular subset might be important for the generation of anti-*Pf*GARP antibodies. Interestingly, activated $cT_{FH}1$-like (MC06) and quiescent $cT_{FH}1$-like (MC07) cells were more abundant for adults with low or no anti-*Pf*GARP IgG antibodies compared to those with high levels (p=0.0024 with FDR=0.0185 and p=0.0034 with FDR=0.0185, respectively) consistent with previous observations describing $T_{FH}1$ subsets as inefficient help for antibody production[29].

Discussion

The overall aim of this study was to define cT_{FH} subsets using unbiased clustering analysis and assess their malaria antigen-specific (*Pf*SEA-1A and *Pf*GARP)[6,7,39] profiles for adults and children residing in a malaria-holoendemic area of Kenya. Contrary to previous publications,[29,30] our study found that children not only respond via their $cT_{FH}1$-like subsets but also engage a broader spectrum of cT_{FH} subsets. In fact, cytokine and transcription factor profiles for children involved $cT_{FH}1$-, $cT_{FH}2$-, $cT_{FH}17$-, and $cT_{FH}1/17$-like subsets (summarized in Figure 9), whereas in adults, the dominant antigen-specific memory response was from $cT_{FH}17$- and $cT_{FH}1/17$-like subsets but only for *Pf*GARP. Thus, revealing a potential difference in engaging cT_{FH} help between the two malaria vaccine candidates evaluated in this study.

Several key points can be made from our results. First, it may be too soon in the field of cT_{FH} biology to select only one or two types of cT_{FH} subset(s) to measure when evaluating malaria vaccine candidates, especially if we miss essential, albeit transient, correlates of

protection for children which may differ in adults. Longitudinal studies with clinical outcomes are needed to determine the impact of the changing dynamics of cT_{FH} subset adaptations after repeated malaria infections that lead to premunition and parasite clearance. A Ugandan study by Chan et al.[31] demonstrated an age-associated change in cT_{FH} subsets independent of malaria and, thus, supports the importance of accounting for age when evaluating antigen-specific cT_{FH} profiles. Second, our study reveals that adults have a robust cT_{FH}17- and cT_{FH}1/17-like subset response to *Pf*GARP but not to *Pf*SEA-1A. In addition to demonstrating differences between malaria antigens, this finding supports the premise that cT_{FH}17 cells are important for maintaining immunological memory,[40] which has intriguing implications for evaluating malaria vaccine efficacy. Third, we found a correlation between cT_{FH}1or2-like (MC04) and high *Pf*GARP antibodies for both children and adults, indicating that a cT_{FH} subset accompanied by high antibody levels could serve as a potential biomarker of protection. More studies are needed to explore this association; however, we postulate that a coalition of cT_{FH} subsets might be engaged to develop long-lived antibody responses and, therefore, categorizing subsets as efficient or inefficient might be context dependent.[29]

As the field of computational immunology and unbiased clustering analyses evolves, it presents an ongoing challenge to meaningfully define cT_{FH} subsets. Here, we intentionally chose to use cT_{FH}1or2-like nomenclature for meta-clusters MC03, MC04, MC05, and MC08 (Figure 9) because of their low (but not null) CXCR3 and robust IL-4 expression along with Bcl6 and cMAF). CXCR3 expression leans toward a cT_{FH}1-like polarization, whereas IL-4 expression indicates a cT_{FH}2-like profile when we follow the most commonly used cT_{FH} classification.[17,21,22,33] This difference is crucial as cT_{FH}2 cells are described as good promoters for functional GC antibodies[28,30], whereas cT_{FH}1 cells are not.[29,30,41] Therefore, their definitive classification will require a more in-depth investigation. Although we used malaria antigen-specific stimulation, and not a *Pf*-lysate or infected red blood cells (iRBCs)

as previously described,[29–31] adults had significantly more of the quiescent $cT_{FH}2$-like subset (MC02) compared to children who, instead, had significantly more of the activated $cT_{FH}1$-like subset (MC06), the latest being consistent with previous publications,[29,30] and more $PD1^{high}$ activated and $ICOS^{high}$ quiescent $cT_{FH}1or2$-like subsets (MC03 and MC08, respectively). However, even when classifying the cT_{FH} meta-clusters as $cT_{FH}1$, $cT_{FH}2$, $cT_{FH}17$, or $cT_{FH}1/17$, the most abundant cT_{FH} subset was $cT_{FH}2$ cells for adults (more than 50%) contradicting a previous study showing only ~20% of $cT_{FH}2$ cells for the same age range.[31] As suggested by Gowthaman's T_{FH} model,[27] $T_{FH}1$ cells are involved in the development of neutralization antibody responses to viruses and bacteria, whereas parasites, such as helminths, lead to a $T_{FH}2$ response. These observations reinforce the need to assess T_{FH} subset profiles stratified by exposure to potentially immune-modulating co-infections.

Transcription factors cMAF and Bcl6 play essential roles in T_{FH} development and function.[24,42,43] cMAF induces the expression of various molecules, such as ICOS, PD1, CXCR5, IL-4, and IL-21, which are all essential for T_{FH} function.[42] It was, therefore, not surprising to find that cMAF significantly increased after antigen stimulation for most of the cT_{FH} subsets in children. However, again, this expression profile was only observed in the activated $cT_{FH}1/17$-like subset (MC11) after *Pf*GARP stimulation in cells from adults, supporting a role for $T_{FH}17$ cells in the maintenance of immunological memory.[40] Importantly, cMAF cooperates with Bcl6 in T_{FH} development and function and is essential to establish an efficient GC response.[24,44] Bcl6 is also described as being expressed by mature T_{FH} cells, inducing the expression of CXCR5 and PD1, but it can also regulate IFNγ and IL-17 production.[12,24,44,45] In our study, *Pf*GARP induced a highly significant increase of Bcl6 in $cT_{FH}2$-like and $cT_{FH}17$-like subsets in children, suggesting that *Pf*GARP may be a better candidate to trigger an efficient humoral response in children compared to *Pf*SEA-1A. Of

note, Blimp1, a Bcl6 antagonist,[45] was absent from our flow panel and would be of interest to assess in future studies.

There are several limitations of human immune profiling studies. Similar to other such studies, we used peripheral blood and, thus, were only able to provide a snapshot of the cT_{FH} cells. Study participants did not have blood-stage malaria infections at the time of blood collection, and children were 7 years of age; thus, our profiles were by design meant to reflect cT_{FH} memory recall responses and demonstrate differences between children and adults. As this was not a birth cohort study design, the number of cumulative malaria infections could have confounded the association between malaria and cT_{FH} subsets, causing a certain cT_{FH} meta-cluster to arise. Most human immunology studies are unable to assess tissue-resident T_{FH} or T_{FH} in the lymph nodes. Therefore, we can only speculate on the composition of T_{FH} cells observed in children that were perhaps short-lived helper cells and not maintained as T cell memory cells or may have trafficked from the blood into tissues over time.[46] Using an *in vivo* non-human primate model, Potter et al., showed an entry rate of lymphocyte subsets into peripheral lymph nodes per hour of 1.54% and 2.17% for $CD4^{pos}$ central memory ($CD45^{neg}CCR7^{pos}$) and effector memory ($CD45^{neg}CCR7^{neg}$) T cells, respectively,[46] both of which may include central and effector memory cT_{FH} cells. With this in mind, cT_{FH} cells seem to be at a crossroads with multiple possible fates. The first one being the recirculation of cT_{FH} cells from lymph node to lymph node, whereby a peripheral blood sampling captures migratory cT_{FH} subsets, which could explain the cT_{FH} subsets we observed still expressing cMAF and Bcl6. A decade ago, it was hypothesized that once a T_{FH} cell leaves the lymph node, it can become a $PD1^{low}$ memory cT_{FH} cell with the possibility of returning to a GC T_{FH} stage after a secondary recall response.[12] Other possible fates include becoming a $PD1^{neg}$ memory cT_{FH} with the same path after recall or progressing to a non-T_{FH} cell.[12] More recently, a few studies showed circulating $CXCR5^{neg}CD4^{pos}$ cells with T_{FH} functions, such as

production of IL-21 and the capability to help B cells in systemic lupus erythematosus and HIV-infected individuals,[47,48] and importantly researchers mapped these circulating $CXCR5^{neg}CD4^{pos}$ cells to an original lymph node $CXCR5^{pos}$ T_{FH} subset,[48] suggesting another possible outcome for T_{FH} cells outside secondary lymphoid organs. To date, no clear destiny has been established for cT_{FH} cells in humans, thus, highlighting the importance of including a complete panel of cT_{FH} subsets to continue to improve our understanding of their respective roles against different pathogens and eliciting long-lived vaccine-induced antibody responses.

Other limitations of this study include not measuring other cytokines (i.e., IL-5, IL-13, and IL-17) and transcription factors (i.e., T-bet, BATF, GATA3, and RORγt) that have been used in other studies to fully characterize cT_{FH} subsets[12,27]. Although the heterogeneity in the response of CD40L and IFNγ suggests that our tested malaria antigens did not induce significant differences in the expression of these markers in all our participants, our panel did not include other activated induced markers, such as OX40, 4-1BB, and CD69. However, even with our small sample size, we demonstrated significant age-associated differences in malaria antigen-specific responses from different cT_{FH} subsets. To minimize false-positive results that can arise when using algorithms for computational analyses, we ran the statistical tests in triplicate and the clustering algorithm in duplicate, to validate our findings.

In summary, our study provides additional justification for the resources needed to conduct cellular immunological studies of cT_{FH} cell signatures and provides insight into which types of cT_{FH} subsets during a person's lifespan assist B cells in the GC to produce long-lived plasmocytes and functional antibodies[49] against malaria. This is particularly important when selecting immune correlates of protection that could be used to predict the efficacy of the next generation of *Pf*-malaria vaccine candidates within various study populations.

Methods

Study populations and ethical approvals

Adults and children were recruited from Kisumu County, Kenya, which is holoendemic for *Pf*-malaria. Written informed consent was obtained from each adult participant and every child's guardian. An abbreviated medical history, physical examination, and blood film were used to ascertain health and malaria infection status at the time of blood sample collection. Participants were also life-long residents of the study area with an assumption that they naturally acquired immunity to malaria. This study was conducted before the implementation of any malaria vaccines. Participants were eligible if they were healthy and not experiencing any symptoms of malaria at the time venous blood was collected. For this cross-sectional immunology study, we selected fourteen 7-year-old children from a larger age-structured prospective cohort study (enrollment age range 3–7 years) and fifteen Kenyan adults. We selected 7-year-olds because of the age-dependent shift in major cT_{FH} subsets occurring after 6 years of age[31], and as a comparable age published by other studies[29], to maximize our ability to measure antigen-specific differences in T_{FH} subsets.

Ethical approvals were obtained from the Scientific and Ethics Review Unit (SERU) at the Kenya Medical Research Institute (KEMRI) reference number 3542, and the Institutional Review Board at the University of Massachusetts Chan Medical School, Worcester, MA, USA, IRB number H00014522. Brown University, Providence, RI, USA signed a reliance agreement with KEMRI.

Plasma and peripheral blood mononuclear cell (PBMC) isolation

Venous blood was collected in sodium heparin BD Vacutainers and processed within 2 hours at the Center for Global Health Research, KEMRI, Kisumu. Absolute lymphocyte counts (ALC) were determined from whole blood using BC-3000 Plus Auto Hematology Analyzer, 19 parameters (Shenzhen Mindray Bio-Medical Electronics Co.). After 10 mins at 1,000*g*

spin, plasma was removed and stored at -20 ^{o}C, and an equivalent volume of 1X PBS was added to the cell pellet. PBMCs were then isolated using Ficoll-Hypaque density gradient centrifugation on SepMate (StemCell). PBMCs were frozen at $5x10^6$ cells/ml in a freezing medium (90% heat-inactivated and filter-sterilized fetal bovine serum [FBS] and 10% dimethyl sulfoxide [DMSO, Sigma]) and chilled overnight in Mr. Frosty™ containers at -80 ^{o}C before being transferred to liquid nitrogen. For transport to the USA, an MVE vapor shipper (MVE Biological Solutions) was used to maintain the cold chain.

In-vitro stimulation assay

PBMCs were thawed in 37 ^{o}C filtered-complete media (10% FBS, 2 mM L-Glutamine, 10 mM HEPES, 1X Penicillin/Streptomycin) and spun twice before resting overnight in a 37 ^{o}C, 5% CO_2 incubator. PBMCs were counted using Trypan Blue (0.4%) and a hemocytometer, and the cell survival was calculated. Our samples showed a median of 94.6% live cells (25% percentile of 92%; 75% percentile of 97%). Using a P96 U-bottom plate, $1x10^6$ PBMCs per well were placed in culture with one of the following stimulation conditions: *Pf*SEA-1A[6] (5 µg/ml) or *Pf*GARP[7] (10 µg/ml) both produced in the Kurtis lab (Brown University); SEB (1 µg/ml; EMD Millipore) was used as a positive control; sterile water (10 µl, the same volume used to reconstitute *Pf*SEA and *Pf*GARP) was used as a negative control. A pool of anti-CD28/anti-CD49d (BD Fast-Immune Co-Stim following the manufacturer's instructions), GolgiSTOP (0.7 µg/ml), and GolgiPLUG (0.1 µg/ml) (BD Biosciences) were added to each well before incubating cells at 37 ^{o}C for 6 hours.

Cell staining and flow cytometry

A multiparameter spectral flow cytometry panel was used to characterize cT_{FH} cell subsets: CCR6-BV421 (RRID: AB_2561356), CD14-Pacific Blue (RRID: AB_830689), CD19-Pacific Blue (RRID: AB_2073118), CCR7-BV480 (RRID: AB_2739502), IFNγ-BV510 (RRID: AB_2563883), CD127-BV570 (RRID: AB_10900064), CD45RA-BV605 (RRID:

AB_2563814), PD1-BV650 (RRID: AB_2738746), CXCR3-BV711 (RRID: AB_2563533), CD25-BV750 (RRID: AB_2871896), CXCR5-BV785 (RRID: AB_2629528), Bcl6-AF488 (RRID: AB_10716202), CD3-Spark Blue 550 (RRID: AB_2819985), CD8-PerCP-Cy5.5 (RRID: AB_2044010), IL-21-PE (RRID: AB_2249025), IL-4-PE-Dazzle (RRID: AB_2564036), CD4-PE-Cy5 (RRID: AB_314078), ICOS-PE-Cy7 (RRID: AB_10643411), cMAF-eFluor 660 (RRID: AB_2574388), CD40L-AF700 (RRID: AB_2750053), and Zombie NIR (BioLegend cat# 423106) for Live/Dead staining. Cells were fixed and permeabilized for 45 mins using the transcription factor buffer set (BD Pharmingen) followed by a wash with the perm-wash buffer. Intracellular staining was performed at 4 ^{o}C for 45 more mins followed by two washes using the kit's perm-wash buffer. Data was acquired on a Cytek Aurora with 4-lasers (UMass Chan Flow Core Facility) using SpectroFlo® software (Cytek) and compensation for unmixing and fluorescence-minus-one controls. Quality control of the data was performed using SpectroFlo®, and the multi-parameter analysis was performed with OMIQ data analysis software (www.omiq.ai). Thus, we assessed the expression of markers commonly used to define the following different cT_{FH} ($CD4^{pos}CD25^{neg}CXCR5^{pos}$) subsets: $cT_{FH}1$-like ($CCR6^{neg}CXCR3^{pos}$), $cT_{FH}2$-like ($CCR6^{neg}CXCR3^{neg}$), and $cT_{FH}17$-like ($CCR6^{pos}CXCR3^{neg}$),[17] as well as quiescent/central memory cT_{FH} ($CCR7^{high}PD\text{-}1^{neg}ICOS^{neg}$) or activated/effector memory cT_{FH} cells ($CCR7^{low}PD\text{-}1^{pos}ICOS^{pos}$).[17,18] Representative cytoplots can be found in Supplemental Figure 1.

Multiplex suspension bead-based serology assay

To measure plasma IgG antibody levels to *Pf*SEA-1A[6] and *Pf*GARP[7], we used a Luminex bead-based suspension assay as previously published.[50,51] In addition, previous *Pf* exposure was determined using recombinant proteins to blood-stage malaria antigens: AMA1, MSP1, HRP2, CelTos, and CSP (gifts from Sheetji Dutta, Evelina Angov, and Elke Bergmann from

the Walter Reed Army Institute of Research). Briefly, 100 μg of each antigen or BSA (Sigma), as a background control, were coupled to ~$12x10^6$ non-magnetic microspheres (Bio-Rad carboxylated beads) and then incubated with study participant plasma (spun down 10,000*g* for 10 mins and diluted at 1:100 in the assay dilution buffer) for 2 hrs, followed by incubation with biotinylated anti-human IgG (BD #555785) diluted 1:1000 for 1 hr and streptavidin (BD #554061) diluted 1:1000 for 1 hr following the manufacturer's instructions. The mean fluorescence intensity (MFI) of each conjugated bead (minimum of 50 beads per antigen) was quantified on a FlexMap3D Luminex multianalyte analyzer (Xponent software). Results are reported as antigen-specific MFI after subtracting the BSA value for each individual since background levels can vary between individuals.

OMIQ analysis

The fcs files were uploaded into the OMIQ platform after passing quality control under SpectroFlo® (Cytek) where compensation was re-checked. In OMIQ, we arcsinh-transformed the scale to allow downstream analysis and then gated on singlet live lymphocytes and sub-sampled the data to yield 87,712 live lymphocytes per sample. Using only lineage markers CD3, CD4, CD8, CD14, CD19, CXCR5, and CD25, FlowSOM consensus meta-clustering was run on 100 clusters based on the 87,712 live lymphocytes per sample with a comma-separated k-value of 75 and Euclidean distance metric. Using these 75 meta-clusters, we defined subsets of cells based on lineage markers, such as $CD3^{pos}CD8^{pos}$, $CD3^{neg}CD14^{pos}CD19^{pos}$, and $CD3^{pos}CD4^{pos}$, and then distinguished $CD4^{pos}CXCR5^{pos}CD25^{neg}$ (cT_{FH}) and $CD4^{pos}CXCR5^{neg}CD25^{pos}$ (T regulatory [T_{reg}] or T follicular regulatory [T_{FR}]) subsets. CD25 was used to exclude T_{reg} and T_{FR} cells which share numerous markers with cT_{FH} cells.[52–54] EmbedSOM dimensional reduction was used to visualize the different groups of cells and EdgeR analysis was run to assess the significance of their differences. A

clustering heatmap was used to visualize cytokine expression and transcription factor profiles for each subset.

Focusing on the $CD4^{pos}CXCR5^{pos}CD25^{neg}$ T_{FH} cells, we ran another FlowSOM analysis based on the 1,000 $CXCR5^{pos}$ cells per sample (two samples from the adult group and one sample from the children group were excluded from the analysis as they had less than 1,000 $CXCR5^{pos}$ cells), using extracellular markers CXCR5, CXCR3, CCR6, ICOS, CCR7, CD45RA, CD127, CD40L, and PD1 enabled the identification of 15 meta-clusters. If the fcs file had more than 1,000 $CXCR5^{pos}$ cells, the down-sampling was done randomly by the OMIQ platform algorithm to select only 1,000 $CXCR5^{pos}$ cells within this specific fcs file. From there, we performed Uniform Manifold Approximation and Projection (UMAP) dimensional reduction, heatmaps, and EdgeR analyses; the latter allowed statistical analysis of the cT_{FH} abundances. To demonstrate the reproducibility of these results, statistical analysis algorithms were run at least three times downstream of the same clustering algorithm and downstream of repeated clustering algorithms. To assess statistical differences in cytokines and transcription factor expression, we exported the statistics dataset from OMIQ containing MFI values from each marker (IFN□, IL-4, IL-21, Bcl6, and cMAF) per cluster and for each sample and stimulation condition. To assess cytokines and transcription factors without bias, we chose to use the total MFI expression per meta-cluster with the assumption that cells with increased production of the desired analyte trigger an increase in the overall meta-cluster MFI compared to unstimulated cells, and if there is no production of the desired analyte, the overall MFI will not differ. However, the percentage of positive IFN□, IL-4, IL-21, Bcl6, or cMAF using manual gating can be found in Supplemental Figures 14, 15, and 16 along with the overlay of the gated positive cells on the $CD4^{pos}CXCR5^{pos}CD25^{neg}$ UMAP and the cytoplots of the gated positive cells for each meta-cluster (Supplemental Figures 14, 15, and 16).

Statistical analysis

For this cross-sectional immunology study, we selected both male and female study participants (sex defined at birth). There were fourteen 7-year-old children and fifteen adults. Using GraphPad Prism software (version 7.0), age, sex, ALC, and serological data were compared between adults and children. Because the number of participants within each group was too low to verify the normality of the underlying distributions (adults n=15 and children n=14), we chose to use non-parametric tests, including the Mann-Whitney U test (for unpaired analysis) and Wilcoxon signed-rank test (for paired analysis). When data passed the normality test (D'Agostino and Pearson test), we used Welch's parametric test. All tests were two-tailed with a *p-value* < 0.05 for significance. Because of the exploratory nature of the analysis, we did not use any adjustment of the *p*-value for multiple comparisons. The tests used are indicated in the legend of each figure. Results were expressed as the mean with standard deviation and exact *p*-values for dot plots.

To perform a statistical analysis of the cytokine and transcription factor expression from each cT_{FH} subset, the exported data file from OMIQ was integrated into GraphPad Prism, and a non-parametric Wilcoxon paired two-tailed *t*-test analysis was done (n=13 in each group). As this analysis generated numerous bar plots (all included in the Supplemental Figures 12 to 15), to better visualize the cytokines and transcription factor patterns, the *p*-values obtained from each analysis are presented using a non-clustering heatmap.

Role of the funding source

The funders were not involved in the study design, sample collection, data analysis, interpretation of the data, or the writing of the manuscript and its decision to be submitted for publication.

Contributors

CN, JMO, JK, and AMM designed the research study; CF and SPT conducted experiments; CF, JK, and AMM analyzed data; CF, SPT, JK, and AMM contributed to experimental design; HWW, BO, JMO, JK, and AMM conducted and supervised the clinical study and the sampling; CF generated figures; HWW and BO verified underlying data; CF and AMM led manuscript preparation with feedback from all the authors. All authors have read and approved the final version of the manuscript.

Data Availability

Deidentified raw data from this manuscript are available from the ImmPort platform under the accession study number SDY2534.

Declaration of Competing Interest

Dr. Kurtis was the principal investigator on 1R01AI127699-01A1, which supported this study. He holds several patents related to the use of *Pf*SEA-1 and *Pf*GARP as vaccine candidates for *P. falciparum* and has consulted for and is an equity holder in Ocean Biomedical.

Acknowledgments

The authors would like to thank the children and their families for participating in this study. We thank the field and lab teams for their work collecting data and processing blood samples. We also thank Dr. Melanie Trombly from UMass Chan for proofreading our manuscript. This manuscript was approved for publication by KEMRI.

This study was supported by NIH R01 AI127699 (Kurtis).

References

1. Geneva: World Health Organization. World malaria report 2022. WHO; 2022. Report No.: Licence: CC BY-NC-SA 3.0 IGO.

2. Taylor SM, Juliano JJ. Artemisinin combination therapies and malaria parasite drug resistance: the game is afoot. J Infect Dis. 2014 Aug 1;210(3):335–7.

3. Aydemir O, Janko M, Hathaway NJ, Verity R, Mwandagalirwa MK, Tshefu AK, et al. Drug-Resistance and Population Structure of Plasmodium falciparum Across the Democratic Republic of Congo Using High-Throughput Molecular Inversion Probes. J Infect Dis. 2018 Aug 14;218(6):946–55.

4. Ippolito MM, Moser KA, Kabuya JBB, Cunningham C, Juliano JJ. Antimalarial Drug Resistance and Implications for the WHO Global Technical Strategy. Curr Epidemiol Rep. 2021 Mar 14;8(2):46–62.

5. RTS,S Clinical Trials Partnership. Efficacy and safety of RTS,S/AS01 malaria vaccine with or without a booster dose in infants and children in Africa: final results of a phase 3, individually randomised, controlled trial. Lancet. 2015 Jul 4;386(9988):31–45.

6. Raj DK, Nixon CP, Nixon CE, Dvorin JD, DiPetrillo CG, Pond-Tor S, et al. Antibodies to PfSEA-1 block parasite egress from RBCs and protect against malaria infection. Science. 2014 May 23;344(6186):871–7.

7. Raj DK, Das Mohapatra A, Jnawali A, Zuromski J, Jha A, Cham-Kpu G, et al. Anti-PfGARP activates programmed cell death of parasites and reduces severe malaria. Nature. 2020 Jun;582(7810):104–8.

8. Nixon CE, Park S, Pond-Tor S, Raj D, Lambert LE, Orr-Gonzalez S, et al. Identification of Protective B-Cell Epitopes within the Novel Malaria Vaccine Candidate Plasmodium falciparum Schizont Egress Antigen 1. Clin Vaccine Immunol [Internet]. 2017 Jul;24(7). Available from: http://dx.doi.org/10.1128/CVI.00068-17

9. Holder AA. Malaria vaccines. Proc Natl Acad Sci U S A. 1999 Feb 16;96(4):1167–9.

10. Amanna IJ, Carlson NE, Slifka MK. Duration of humoral immunity to common viral and vaccine antigens. N Engl J Med. 2007 Nov 8;357(19):1903–15.

11. Tarlinton D, Good-Jacobson K. Diversity among memory B cells: origin, consequences, and utility. Science. 2013 Sep 13;341(6151):1205–11.

12. Crotty S. T follicular helper cell differentiation, function, and roles in disease. Immunity. 2014 Oct 16;41(4):529–42.

13. Crotty S. T Follicular Helper Cell Biology: A Decade of Discovery and Diseases. Immunity. 2019 May 21;50(5):1132–48.

14. Breitfeld D, Ohl L, Kremmer E, Ellwart J, Sallusto F, Lipp M, et al. Follicular B helper T cells express CXC chemokine receptor 5, localize to B cell follicles, and support immunoglobulin production. J Exp Med. 2000 Dec 4;192(11):1545–52.

15. Crotty S. Follicular helper CD4 T cells (TFH). Annu Rev Immunol. 2011;29:621–63.

16. He J, Tsai LM, Leong YA, Hu X, Ma CS, Chevalier N, et al. Circulating precursor CCR7(lo)PD-1(hi) CXCR5^{+} CD4^{+} T cells indicate Tfh cell activity and promote antibody responses upon antigen reexposure. Immunity. 2013 Oct 17;39(4):770–81.

17. Schmitt N, Bentebibel SE, Ueno H. Phenotype and functions of memory Tfh cells in human blood. Trends Immunol. 2014 Sep;35(9):436–42.

18. Gong F, Zheng T, Zhou P. T Follicular Helper Cell Subsets and the Associated Cytokine IL-21 in the Pathogenesis and Therapy of Asthma. Front Immunol. 2019 Dec 13;10:2918.

19. Dunham RM, Cervasi B, Brenchley JM, Albrecht H, Weintrob A, Sumpter B, et al. CD127 and CD25 expression defines CD4+ T cell subsets that are differentially depleted during HIV infection. J Immunol. 2008 Apr 15;180(8):5582–92.

20. Bélanger S, Crotty S. Dances with cytokines, featuring TFH cells, IL-21, IL-4 and B cells. Nat Immunol. 2016 Sep 20;17(10):1135–6.

21. Seth A, Craft J. Spatial and functional heterogeneity of follicular helper T cells in autoimmunity. Curr Opin Immunol. 2019 Dec;61:1–9.

22. Olatunde AC, Hale JS, Lamb TJ. Cytokine-skewed Tfh cells: functional consequences for B cell help. Trends Immunol. 2021 Jun;42(6):536–50.

23. Andris F, Denanglaire S, Anciaux M, Hercor M, Hussein H, Leo O. The Transcription Factor c-Maf Promotes the Differentiation of Follicular Helper T Cells. Front Immunol. 2017 Apr 27;8:480.

24. Nurieva RI, Chung Y, Martinez GJ, Yang XO, Tanaka S, Matskevitch TD, et al. Bcl6 mediates the development of T follicular helper cells. Science. 2009 Aug 21;325(5943):1001–5.

25. Nurieva RI, Chung Y. Understanding the development and function of T follicular helper cells. Cell Mol Immunol. 2010 May;7(3):190–7.

26. Liu X, Nurieva RI, Dong C. Transcriptional regulation of follicular T-helper (Tfh) cells. Immunol Rev. 2013 Mar;252(1):139–45.

27. Gowthaman U, Chen JS, Zhang B, Flynn WF, Lu Y, Song W, et al. Identification of a T follicular helper cell subset that drives anaphylactic IgE. Science [Internet]. 2019 Aug 30;365(6456). Available from: http://dx.doi.org/10.1126/science.aaw6433

28. Chan JA, Loughland JR, de Labastida Rivera F, SheelaNair A, Andrew DW, Dooley NL, et al. Th2-like T Follicular Helper Cells Promote Functional Antibody Production during Plasmodium falciparum Infection. Cell Rep Med. 2020 Dec 22;1(9):100157.

29. Obeng-Adjei N, Portugal S, Tran TM, Yazew TB, Skinner J, Li S, et al. Circulating Th1-Cell-type Tfh Cells that Exhibit Impaired B Cell Help Are Preferentially Activated during Acute Malaria in Children. Cell Rep. 2015 Oct 13;13(2):425–39.

30. Oyong DA, Loughland JR, Soon MSF, Chan JA, Andrew D, Wines BD, et al. Adults with Plasmodium falciparum malaria have higher magnitude and quality of circulating

T-follicular helper cells compared to children. EBioMedicine. 2022 Jan;75:103784.

31. Chan JA, Loughland JR, de la Parte L, Okano S, Ssewanyana I, Nalubega M, et al. Age-dependent changes in circulating Tfh cells influence development of functional malaria antibodies in children. Nat Commun. 2022 Jul 18;13(1):4159.

32. Stanisic DI, McCall MBB. Correlates of malaria vaccine efficacy. Expert Rev Vaccines. 2021 Feb;20(2):143–61.

33. Bentebibel SE, Jacquemin C, Schmitt N, Ueno H. Analysis of human blood memory T follicular helper subsets. Methods Mol Biol. 2015;1291:187–97.

34. Wei Y, Feng J, Hou Z, Wang XM, Yu D. Flow cytometric analysis of circulating follicular helper T (Tfh) and follicular regulatory T (Tfr) populations in human blood. Methods Mol Biol. 2015;1291:199–207.

35. Pluncevic Gligoroska J, Gontarev S, Dejanova B, Todorovska L, Shukova Stojmanova D, Manchevska S. Red Blood Cell Variables in Children and Adolescents regarding the Age and Sex. Iran J Public Health. 2019 Apr;48(4):704–12.

36. Yman V, White MT, Asghar M, Sundling C, Sondén K, Draper SJ, et al. Antibody responses to merozoite antigens after natural Plasmodium falciparum infection: kinetics and longevity in absence of re-exposure. BMC Med. 2019 Jan 30;17(1):22.

37. O'Flaherty K, Oo WH, Zaloumis SG, Cutts JC, Aung KZ, Thein MM, et al. Community-based molecular and serological surveillance of subclinical malaria in Myanmar. BMC Med. 2021 May 28;19(1):121.

38. Turnbull LB, Ayodo G, Knight V, John CC, McHenry MS, Tran TM. Evaluation of an ultrasensitive HRP2-based rapid diagnostic test for detection of asymptomatic Plasmodium falciparum parasitaemia among children in western Kenya. Malar J. 2022 Nov 16;21(1):337.

39. Duffy PE, Patrick Gorres J. Malaria vaccines since 2000: progress, priorities, products. NPJ Vaccines. 2020 Jun 9;5(1):48.

40. Gao X, Luo K, Wang D, Wei Y, Yao Y, Deng J, et al. T follicular helper 17 (Tfh17) cells are superior for immunological memory maintenance. Elife [Internet]. 2023 Jan 19;12. Available from: http://dx.doi.org/10.7554/eLife.82217

41. Hansen DS, Obeng-Adjei N, Ly A, Ioannidis LJ, Crompton PD. Emerging concepts in T follicular helper cell responses to malaria. Int J Parasitol. 2017 Feb;47(2-3):105–10.

42. Imbratta C, Hussein H, Andris F, Verdeil G. c-MAF, a Swiss Army Knife for Tolerance in Lymphocytes. Front Immunol. 2020 Feb 14;11:206.

43. Liu X, Yan X, Zhong B, Nurieva RI, Wang A, Wang X, et al. Bcl6 expression specifies the T follicular helper cell program in vivo. J Exp Med. 2012 Sep 24;209(10):1841–52, S1–24.

44. Yu D, Rao S, Tsai LM, Lee SK, He Y, Sutcliffe EL, et al. The transcriptional repressor Bcl-6 directs T follicular helper cell lineage commitment. Immunity. 2009 Sep

18;31(3):457–68.

45. Johnston RJ, Poholek AC, DiToro D, Yusuf I, Eto D, Barnett B, et al. Bcl6 and Blimp-1 are reciprocal and antagonistic regulators of T follicular helper cell differentiation. Science. 2009 Aug 21;325(5943):1006–10.

46. Potter EL, Gideon HP, Tkachev V, Fabozzi G, Chassiakos A, Petrovas C, et al. Measurement of leukocyte trafficking kinetics in macaques by serial intravascular staining. Sci Transl Med [Internet]. 2021 Jan 13;13(576). Available from: http://dx.doi.org/10.1126/scitranslmed.abb4582

47. Bocharnikov AV, Keegan J, Wacleche VS, Cao Y, Fonseka CY, Wang G, et al. PD-1hiCXCR5- T peripheral helper cells promote B cell responses in lupus via MAF and IL-21. JCI Insight [Internet]. 2019 Oct 17;4(20). Available from: http://dx.doi.org/10.1172/jci.insight.130062

48. Del Alcazar D, Wang Y, He C, Wendel BS, Del Río-Estrada PM, Lin J, et al. Mapping the Lineage Relationship between CXCR5+ and CXCR5- CD4+ T Cells in HIV-Infected Human Lymph Nodes. Cell Rep. 2019 Sep 17;28(12):3047–60.e7.

49. Moormann AM, Nixon CE, Forconi CS. Immune effector mechanisms in malaria: An update focusing on human immunity. Parasite Immunol. 2019 Aug;41(8):e12628.

50. Cham GKK, Turner L, Lusingu J, Vestergaard L, Mmbando BP, Kurtis JD, et al. Sequential, ordered acquisition of antibodies to Plasmodium falciparum erythrocyte membrane protein 1 domains. J Immunol. 2009 Sep 1;183(5):3356–63.

51. Forconi CS, Cosgrove CP, Saikumar-Lakshmi P, Nixon CE, Foley J, Ong'echa JM, et al. Poorly cytotoxic terminally differentiated CD56negCD16pos NK cells accumulate in Kenyan children with Burkitt lymphomas. Blood Adv. 2018 May 22;2(10):1101–14.

52. Wing JB, Tekgüç M, Sakaguchi S. Control of Germinal Center Responses by T-Follicular Regulatory Cells. Front Immunol. 2018 Aug 24;9:1910.

53. Sage PT, Alvarez D, Godec J, von Andrian UH, Sharpe AH. Circulating T follicular regulatory and helper cells have memory-like properties. J Clin Invest. 2014 Dec;124(12):5191–204.

54. Zhao X, Jin T, Zheng C, Ma D, Zhang Y. Imbalance of Circulating Tfh/Tfr Cells in Patients With Parkinson's Disease. Front Neurol. 2020 Oct 2;11:572205.

Figure Legends

Figure 1: *Pf*-malaria IgG sero-profiles for children and adults. (a) IgG antibody levels against AMA1, MSP1, HRP2, CelTos, and CSP for children (n=14). The bar plots indicate the mean with SD. (**b)** IgG antibody levels against *Pf*SEA-1A and *Pf*GARP comparing children (n=15) and adults (n=15). The bar plots indicate the mean with SD. Net MFI values are the antigen-specific MFI values minus the BSA background. Mann-Whitney tests were performed.

Figure 2: Cluster visualization of immune cell types and their abundance. (a) A 100-node and 75-meta-cluster FlowSOM tree was generated on live lymphocytes from all our participants (n=29 children and adults), highlighting $CD3^{pos}CD8^{pos}$, $CD3^{pos}CD4^{pos}$, $CD4^{pos}CXCR5^{pos}$, and $CD4^{pos}CD25^{pos}$ cells. The 5 nodes of the $CD4^{pos}CXCR5^{pos}CD25^{neg}$ population are circled and were used for the downstream analysis. The colored scale was based on the median arcsinh-transformed marker expression. UMAP plots showing 5 clusters defined as follows: $CD14^{pos}$ and $CD19^{pos}$ (orange), $CD4^{pos}$ (blue), $CD4^{pos}CXCR5^{pos}$ (red), $CD8^{pos}$ (purple), and $CD4^{pos}CD25^{pos}$ (green) from PBMCs isolated from **(b)** adults (n=15) and **(c)** children (n=14) that were unstimulated, stimulated with *Pf*SEA-1A, or stimulated with *Pf*GARP, respectively, from left to right.

Figure 3: Characterization of T_{FH} subsets by CXCR5, CXCR3, CCR6, and CD45RA expression. (a) A new 25-node and 15 meta-cluster FlowSOM tree was generated from the 5 $CD4^{pos}CXCR5^{pos}CD25^{neg}$ nodes shown in Figure 2A (CXCR5 expression tree). The colored scale of CXCR5 expression was based on the median arcsinh-transformed with red as the highest and deep blue as the absence of CXCR5 expression. **(b)** Box plots showing CXCR5 expression across all cT_{FH}-like meta-clusters from children (n=13) with no stimulation (blue), and after *in vitro* stimulation with *Pf*GARP (green) or *Pf*SEA-1A (pink). Fifty percent of the data points are within the box limits, the solid line indicates the median, the dashed line indicates the mean, and the whiskers indicate the range of the remaining data with outliers being outside that range. Similar box plots are shown for **(c)** CD45RA, **(d)** CXCR3, and **(e)** CCR6 expression across all cT_{FH}-like meta-clusters. **(f)** Clustered heatmap showing the median arcsinh-transformed expression for CCR6, CD45RA, CXCR3, and CXCR5 across meta-clusters, red showing the highest expression and blue the lowest. **(g)** Cytoplots of CCR6

vs. CXCR3 expression where MC01 is blue, MC07 is pink, MC11 is yellow, and MC13 is green.

Figure 4: cT_{FH} subset activation state determined by PD1, ICOS, CCR7, and CD127. Box-plots showing **(a)** PD1, **(b)** ICOS, **(c)** CCR7, and **(d)** CD127 expression across all cT_{FH}-like meta-clusters from children (n=13) with no stimulation (blue), and after *in vitro* stimulation with *Pf*GARP (green) or *Pf*SEA-1A (pink). Fifty percent of the data points are within the box limits, the solid line indicates the median, the dashed line indicates the mean, and the whiskers indicate the range of the remaining data with outliers being outside that range.

Figure 5: Differences in abundance of antigen-specific cT_{FH} meta-clusters for adults and children. (a) UMAP plots showing the 12 different cT_{FH} meta-clusters in adults (top three plots, n=13) and in children (bottom three plots, n=13) in the absence of stimulation or after *in vitro* stimulation with *Pf*SEA-1A or *Pf*GARP, from left to right, respectively. Colored circles highlight the meta-clusters showing differences in their abundance between adults and children for each condition. An EdgeR statistical plot was performed to assess the change in abundance of the 12 meta-clusters between adults and children after **(b)** no stimulation or stimulation with **(c)** *Pf*SEA-1A or **(d)** *Pf*GARP. EdgeR plots indicate which meta-clusters are significantly abundant between two groups by using green color dots. The Y-axis is the -$\log_{10}$(*p*-value) and the X-axis is the log(FC). Green dots were statistically significant ($p<0.05$). Numbers next to the dots indicate the meta-cluster. **(e)** An abundance heatmap indicates the percentage (black numbers) of each meta-cluster within the total number of $CD3^{pos}CD4^{pos}CXCR5^{pos}CD25^{neg}$ cells for adults and children (concatenated from 13 participants in each group) under the different conditions: no stimulation (Neg) or stimulation with *Pf*SEA-1A or *Pf*GARP. The color scale ranges from high expression (red) to low/no expression (blue). The star in the heatmap indicates which meta-cluster is significantly abundant in children or adults based on the EdgeR results.

Figure 6: Diverse *Pf*-malaria antigen-specific expression patterns of cT_{FH}-defining cytokines and transcription factors for children. Heatmaps of Wilcoxon-paired two-tailed t-test *p*-values are shown for cT_{FH} meta-clusters comparing **(a)** *Pf*SEA-1A and **(b)** *Pf*-GARP versus unstimulated PBMCs from children (n=13) for each cytokine (IFNγ, IL-4, and IL-21)

and transcription factor (Bcl6 and cMAF). The color scale indicates the significance of the *p*-value: white (non-significant, $p>0.05$), yellow ($0.05>p>0.02$), orange ($0.02>p>0.005$), and red (highly significant, $p<0.005$). The down arrow indicates a decrease of expression from unstimulated to stimulated condition, whereas no arrow indicates an increase of expression from unstimulated to stimulated condition. The cT_{FH} meta-clusters that co-expressed transcription factors were grouped as follows: Group 1 (blue line), Group 2 (green line), and Group 3 (purple line). Bar plots indicating mean with SD of the median intensity fluorescence (MFI) of **(c)** IFNγ, **(d)** Bcl6, and **(e)** cMAF for the cT_{FH} meta-clusters showing significant statistical differences between *Pf*SEA-1A and *Pf*GARP stimulations. The *p*-values from Wilcoxon-paired two-tailed t-tests are indicated.

Figure 7: Limited *Pf*-malaria antigen-specific expression patterns of cT_{FH} defining cytokines and transcription factors for adults. Heatmaps of Wilcoxon-paired two-tailed t-test *p*-values are shown for cT_{FH} meta-clusters comparing **(a)** *Pf*SEA-1A or **(b)** *Pf*-GARP versus unstimulated PBMCs from adults (n=13) for each cytokine (IFNγ, IL-4, and IL-21) and transcription factors (Bcl6 and cMAF). The color scale indicates the significance of the *p*-value: white (non-significant, $p>0.05$), yellow ($0.05>p>0.02$), orange ($0.02>p>0.005$), and red (highly significant, $p<0.005$). The down arrow indicates a decrease of expression from unstimulated to stimulated condition, whereas no arrow indicates an increase of expression from unstimulated to stimulated condition. The only cT_{FH} meta-clusters that expressed transcription factors were in Group 3 (purple box). Bar plots indicate the mean with SD of the median fluorescence intensity (MFI) of **(c)** Bcl6 and (**d**) cMAF for the cT_{FH} meta-clusters showing significant statistical differences between *Pf*SEA-1A and *Pf*GARP stimulations. The *p*-values from Wilcoxon-paired two-tailed t-tests are indicated.

Figure 8: Abundance of cT_{FH} meta-clusters stratified by anti-*Pf*GARP IgG antibody levels. UMAP and EdgeR analyses of **(a)** children (n=13) and **(b)** adults (n=13) where significant differences ($p<0.05$) in the abundance of the cT_{FH} meta-clusters are circled on high versus low *Pf*GARP antibody level (left to right) in the UMAP plot and green dots on the volcano plot (far right).

Figure 9: Summary. Illustration of combined findings showing remarkable differences in cT_{FH} subset abundance and *Pf*-malaria antigen-specific cytokine and transcription factor

responses between children and adults residing in a malaria-holoendemic region of Kenya. Figure created with BioRender.

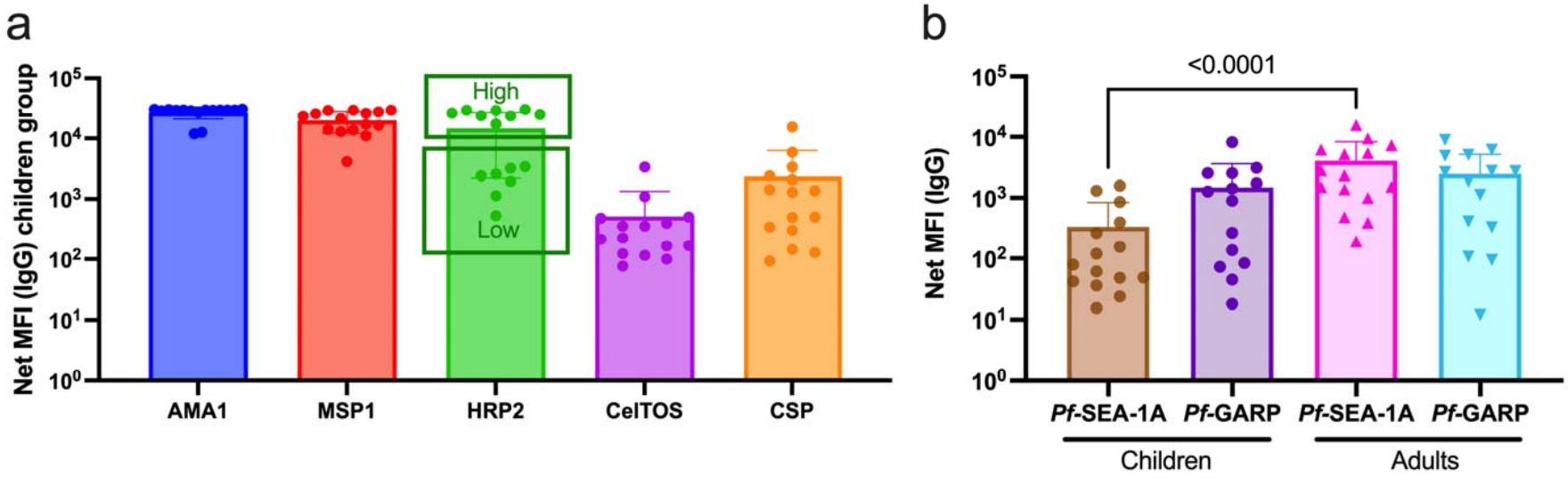
a
Net MFI (IgG) children group
10^5
10^4
10^3
10^2
10^1
10^0
High
Low
AMA1
MSP1
HRP2
CelTOS
CSP
b
Net MFI (IgG)
<0.0001
Pf-SEA-1A
Pf-GARP
Pf-SEA-1A
Pf-GARP
Children
Adults

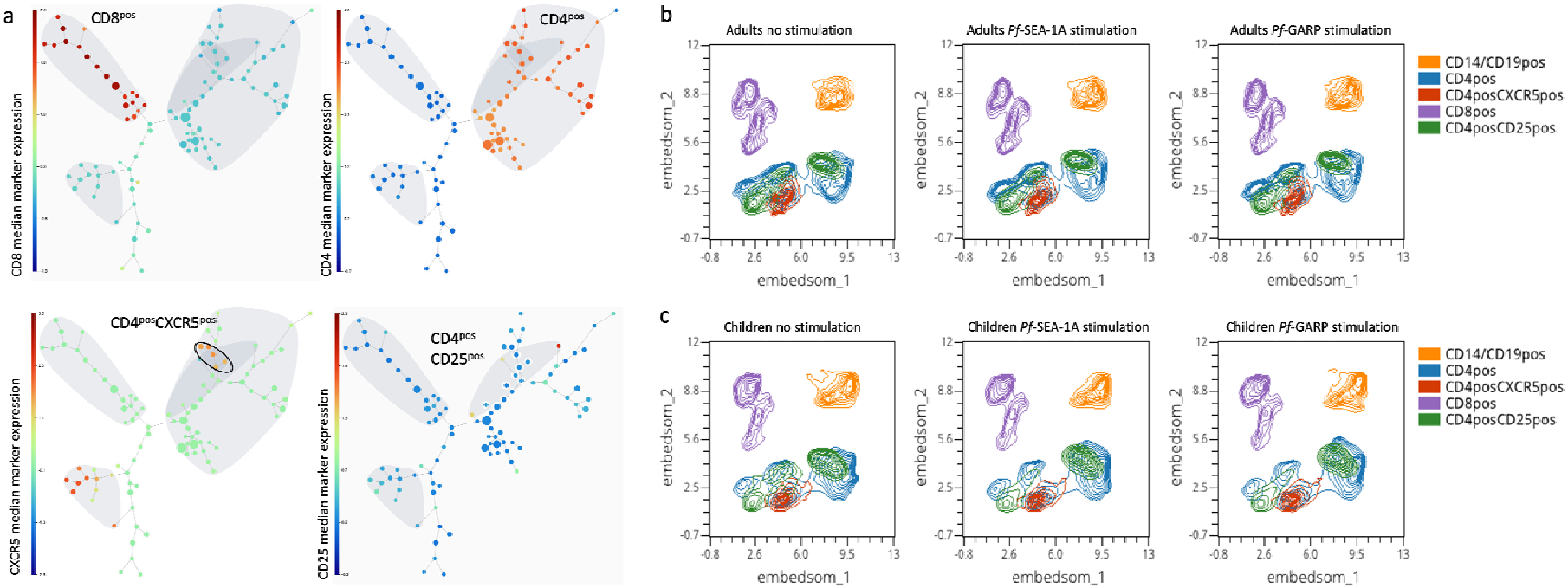
a
CD8pos
CD8 median marker expression
CD4pos
CD4 median marker expression
CD4posCXCR5pos
CXCR5 median marker expression
CD4pos
CD25pos
CD25 median marker expression
b
Adults no stimulation
Adults Pf-SEA-1A stimulation
Adults Pf-GARP stimulation
c
Children no stimulation
Children Pf-SEA-1A stimulation
Children Pf-GARP stimulation
embedsom_1
embedsom_2
CD14/CD19pos
CD4pos
CD4posCXCR5pos
CD8pos
CD4posCD25pos

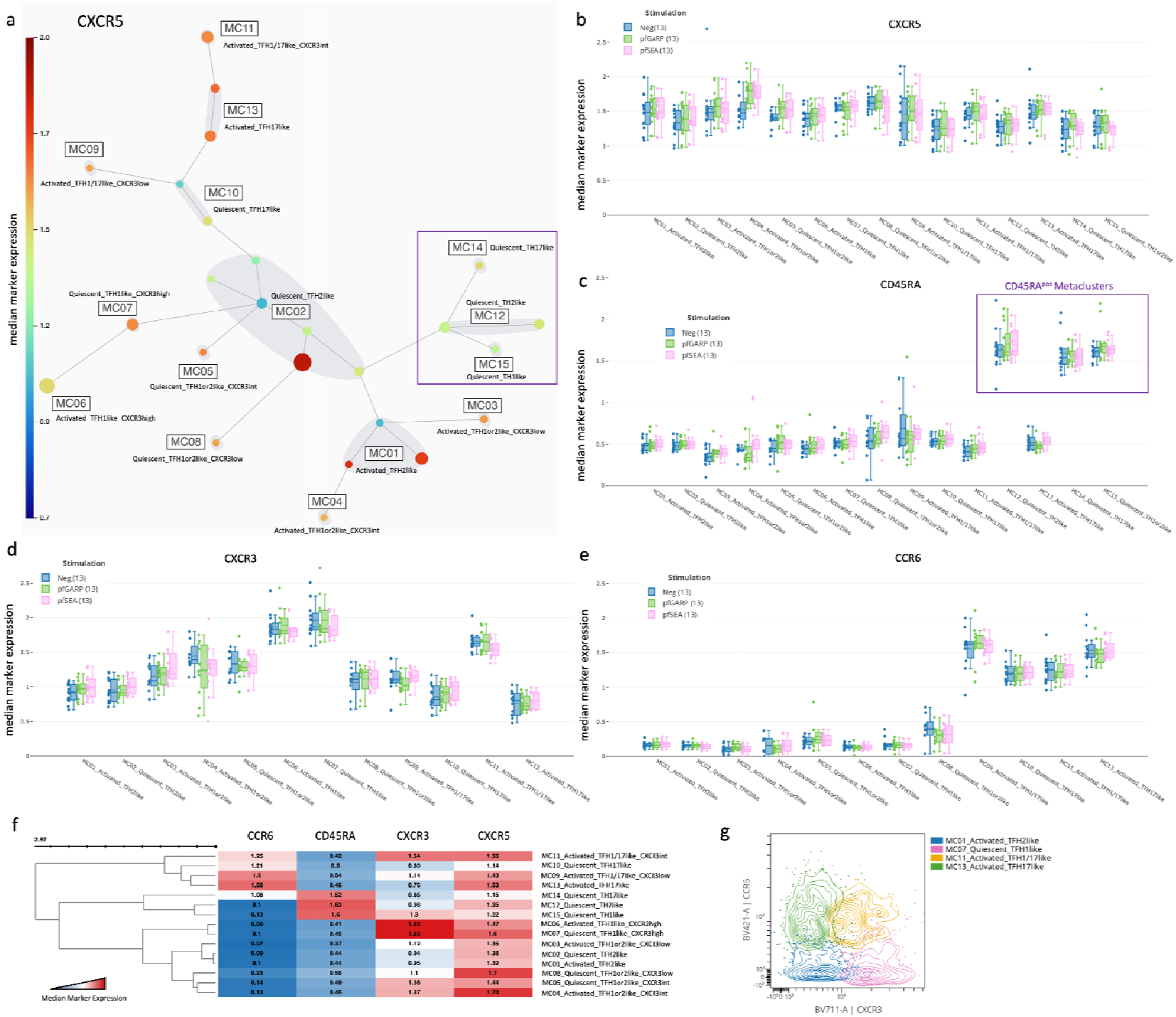
a
CXCR5
median marker expression
MC11
Activated_TFH1/17like_CXCR3int
MC13
Activated_TFH17like
MC09
Activated_TFH1/17like_CXCR3low
MC10
Quiescent_TFH17like
MC14 Quiescent_TH17like
Quiescent_TFH1like_CXCR3high
MC07
Quiescent_TFH2like
MC02
Quiescent_TFH2like
MC12
MC15
Quiescent_TH1like
MC05
Quiescent_TFH1or2like_CXCR3int
MC06
Activated_TFH1like_CXCR3high
MC03
Activated_TFH1or2like_CXCR3low
MC08
Quiescent_TFH1or2like_CXCR3low
MC01
Activated_TFH2like
MC04
Activated_TFH1or2like_CXCR3int
b
CXCR5
Stimulation
Neg(13)
pfGARP (13)
pfSEA (13)
median marker expression
c
CD45RA
CD45RA^pos Metaclusters
Stimulation
Neg (13)
pfGARP (13)
pfSEA (13)
median marker expression
d
CXCR3
Stimulation
Neg(13)
pfGARP (13)
pfSEA (13)
median marker expression
e
CCR6
Stimulation
Neg (13)
pfGARP (13)
pfSEA (13)
median marker expression
f
CCR6
CD45RA
CXCR3
CXCR5
MC11_Activated_TFH1/17like_CXCR3int
MC10_Quiescent_TFH17like
MC09_Activated_TFH1/17like_CXCR3low
MC13_Activated_TFH17like
MC14_Quiescent_TH17like
MC12_Quiescent_TH2like
MC15_Quiescent_TH1like
MC06_Activated_TFH1like_CXCR3high
MC07_Quiescent_TFH1like_CXCR3high
MC03_Activated_TFH1or2like_CXCR3low
MC02_Quiescent_TFH2like
MC01_Activated_TFH2like
MC08_Quiescent_TFH1or2like_CXCR3low
MC05_Quiescent_TFH1or2like_CXCR3int
MC04_Activated_TFH1or2like_CXCR3int
Median Marker Expression
g
MC01_Activated_TFH2like
MC07_Quiescent_TFH1like
MC11_Activated_TFH1/17like
MC13_Activated_TFH17like
BV421-A | CCR5
BV711-A | CXCR3

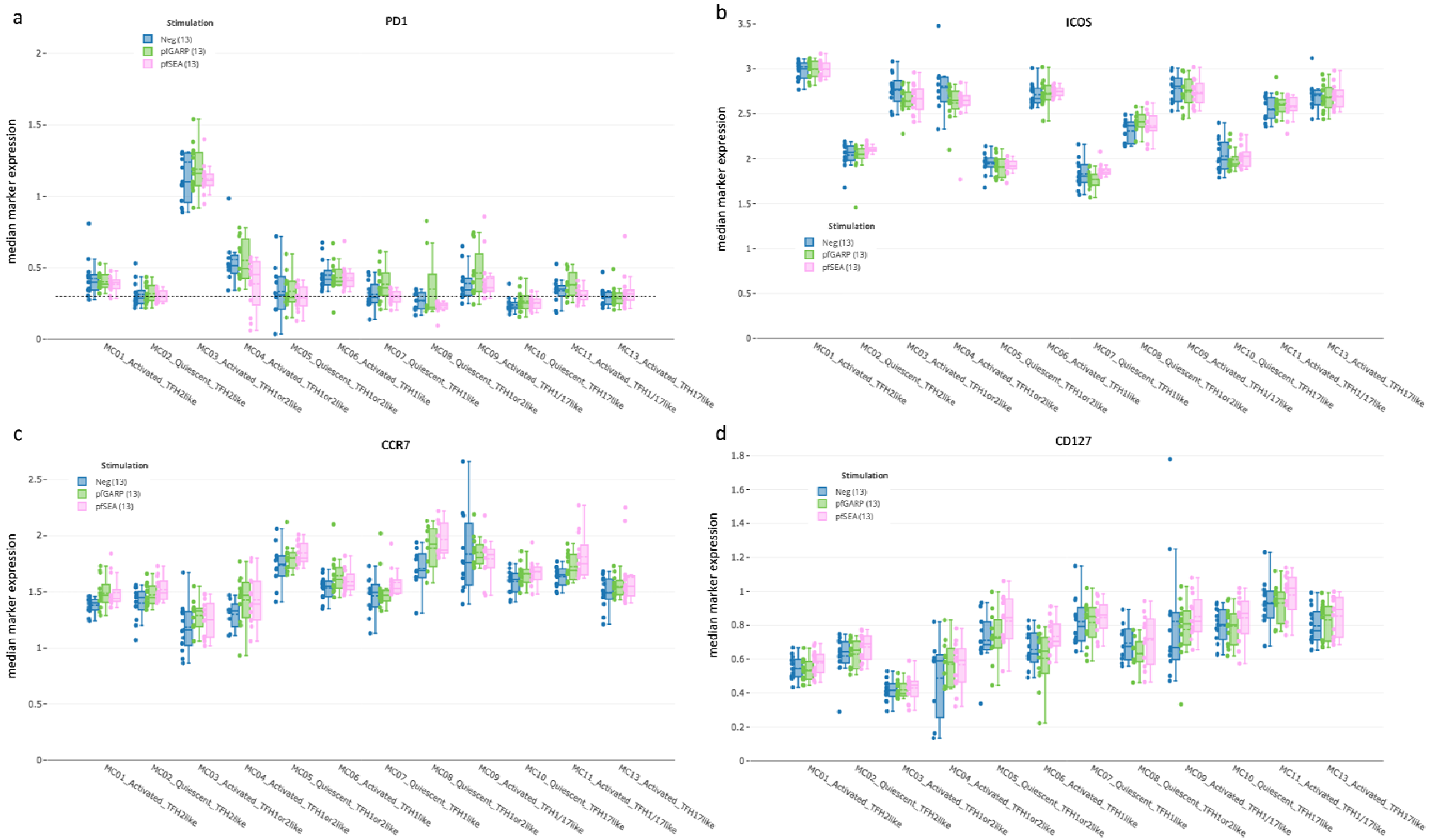
a
PD1
Stimulation
Neg (13)
pfGARP (13)
pfSEA (13)
median marker expression
b
ICOS
c
CCR7
d
CD127
MC01_Activated_TFH2like
MC02_Quiescent_TFH2like
MC03_Activated_TFH1or2like
MC04_Activated_TFH1or2like
MC05_Quiescent_TFH1or2like
MC06_Activated_TFH1like
MC07_Quiescent_TFH1like
MC08_Quiescent_TFH1or2like
MC09_Activated_TFH1/17like
MC10_Quiescent_TFH17like
MC11_Activated_TFH1/17like
MC13_Activated_TFH17like

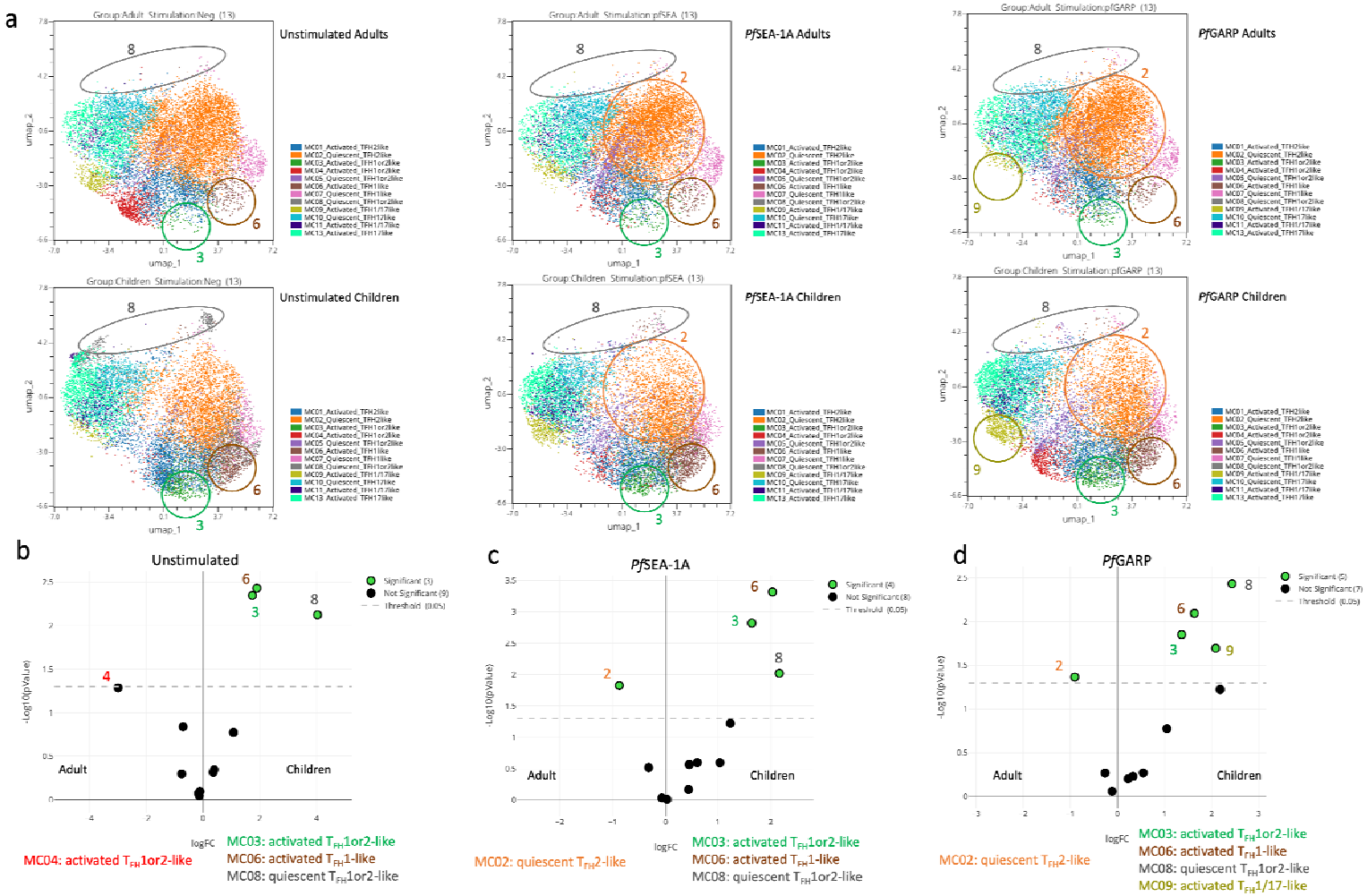

e

	MC01-Act T_{FH}2like	MC02_Qui T_{FH}2like	MC03_Act T_{FH}1or2like	MC04_Act T_{FH}1or2like	MC05_Qui T_{FH}1or2like	MC06_Act T_{FH}1like	MC07_Qui T_{FH}1like	MC08_Qui T_{FH}1or2like	MC09_Act T_{FH}1/17like	MC10_Qui T_{FH}17like	MC11_Act T_{FH}1/17like	MC13_Act T_{FH}17like	Abundance (% of total CD4^{pos}CXCR5^{pos} cells)
Neg	13.4	41.2	0.96	5.48	1.89	2.08	3.42	0.45	2.64	9.18	1.45	7.49	concat_Adult
	16.2	24.1	3.39 *	0.58	1.52	6.64 *	2.88	7.47 *	1.32	8.17	2.88	9.58	concat_Children
PfSEA-1A	13.3	40.9 *	0.94	5.48	1.9	2.02	3.38	0.45	2.65	8.71	1.48	7.85	concat_Adult
	16.3	24.4	3.42 *	0.58	1.52	6.7 *	2.92	7.46 *	1.3	8.65	2.85	9.22	concat_Children
PfGARP	14.8	35.7 *	1.46	5.66	2.12	3.2	3.63	0.63	2.92	8.04	1.72	7.56	concat_Adult
	14.8	29.5	2.89 *	0.4	1.3	5.52 *	2.66	7.28 *	1.04 *	9.32	2.62	9.52	concat_Children

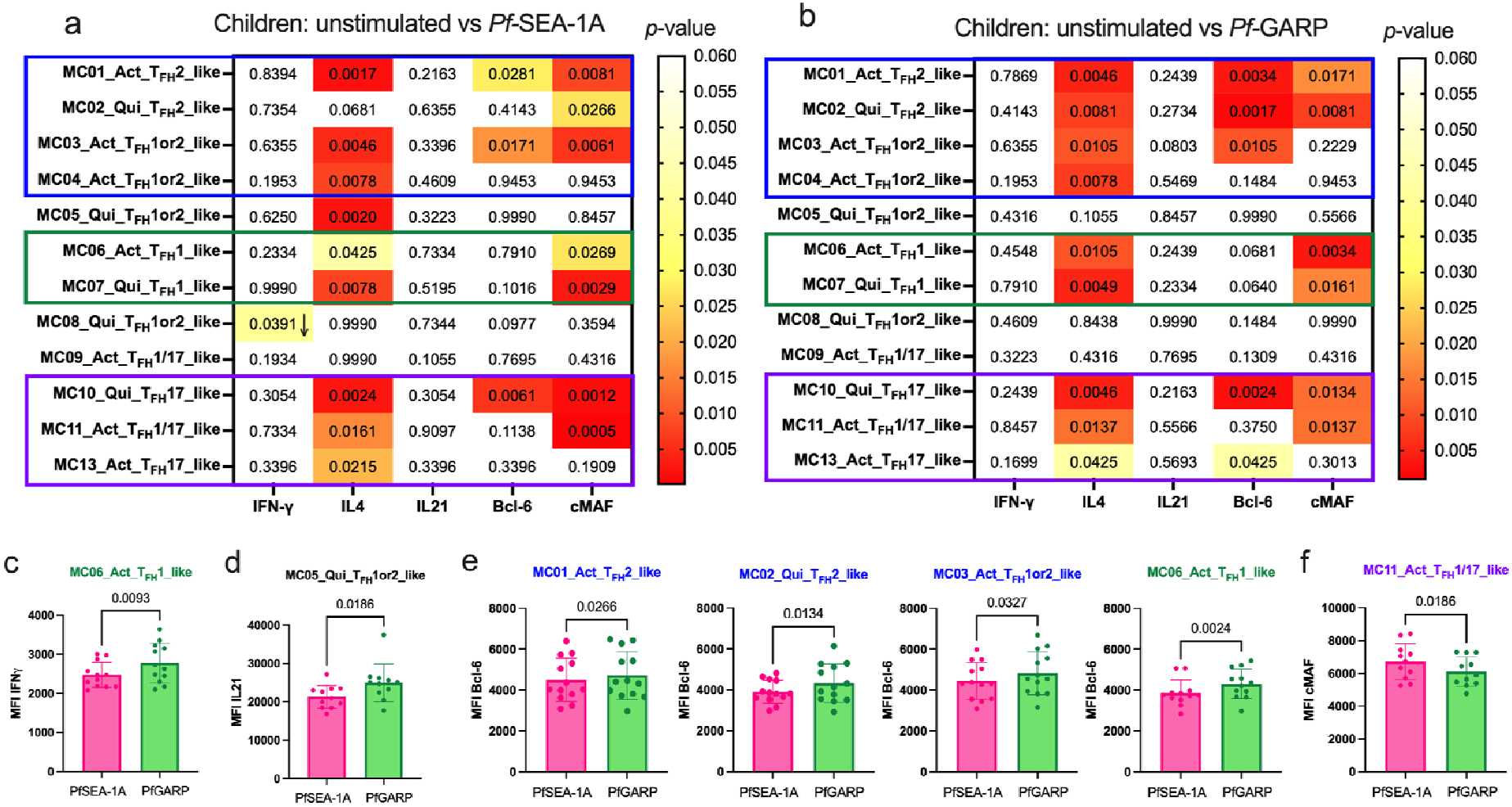
a
Children: unstimulated vs Pf-SEA-1A
p-value
MC01_Act_TFH2_like 0.8394 0.0017 0.2163 0.0281 0.0081
MC02_Qui_TFH2_like 0.7354 0.0681 0.6355 0.4143 0.0266
MC03_Act_TFH1or2_like 0.6355 0.0046 0.3396 0.0171 0.0061
MC04_Act_TFH1or2_like 0.1953 0.0078 0.4609 0.9453 0.9453
MC05_Qui_TFH1or2_like 0.6250 0.0020 0.3223 0.9990 0.8457
MC06_Act_TFH1_like 0.2334 0.0425 0.7334 0.7910 0.0269
MC07_Qui_TFH1_like 0.9990 0.0078 0.5195 0.1016 0.0029
MC08_Qui_TFH1or2_like 0.0391 0.9990 0.7344 0.0977 0.3594
MC09_Act_TFH1/17_like 0.1934 0.9990 0.1055 0.7695 0.4316
MC10_Qui_TFH17_like 0.3054 0.0024 0.3054 0.0061 0.0012
MC11_Act_TFH1/17_like 0.7334 0.0161 0.9097 0.1138 0.0005
MC13_Act_TFH17_like 0.3396 0.0215 0.3396 0.3396 0.1909
IFN-γ IL4 IL21 Bcl-6 cMAF
0.060 0.055 0.050 0.045 0.040 0.035 0.030 0.025 0.020 0.015 0.010 0.005
b
Children: unstimulated vs Pf-GARP
p-value
MC01_Act_TFH2_like 0.7869 0.0046 0.2439 0.0034 0.0171
MC02_Qui_TFH2_like 0.4143 0.0081 0.2734 0.0017 0.0081
MC03_Act_TFH1or2_like 0.6355 0.0105 0.0803 0.0105 0.2229
MC04_Act_TFH1or2_like 0.1953 0.0078 0.5469 0.1484 0.9453
MC05_Qui_TFH1or2_like 0.4316 0.1055 0.8457 0.9990 0.5566
MC06_Act_TFH1_like 0.4548 0.0105 0.2439 0.0681 0.0034
MC07_Qui_TFH1_like 0.7910 0.0049 0.2334 0.0640 0.0161
MC08_Qui_TFH1or2_like 0.4609 0.8438 0.9990 0.1484 0.9990
MC09_Act_TFH1/17_like 0.3223 0.4316 0.7695 0.1309 0.4316
MC10_Qui_TFH17_like 0.2439 0.0046 0.2163 0.0024 0.0134
MC11_Act_TFH1/17_like 0.8457 0.0137 0.5566 0.3750 0.0137
MC13_Act_TFH17_like 0.1699 0.0425 0.5693 0.0425 0.3013
IFN-γ IL4 IL21 Bcl-6 cMAF
0.060 0.055 0.050 0.045 0.040 0.035 0.030 0.025 0.020 0.015 0.010 0.005
c
MC06_Act_TFH1_like
0.0093
MFI IFNγ
PfSEA-1A PfGARP
d
MC05_Qui_TFH1or2_like
0.0186
MFI IL21
PfSEA-1A PfGARP
e
MC01_Act_TFH2_like
0.0266
MFI Bcl-6
PfSEA-1A PfGARP
MC02_Qui_TFH2_like
0.0134
MFI Bcl-6
PfSEA-1A PfGARP
MC03_Act_TFH1or2_like
0.0327
MFI Bcl-6
PfSEA-1A PfGARP
MC06_Act_TFH1_like
0.0024
MFI Bcl-6
PfSEA-1A PfGARP
f
MC11_Act_TFH1/17_like
0.0186
MFI cMAF
PfSEA-1A PfGARP

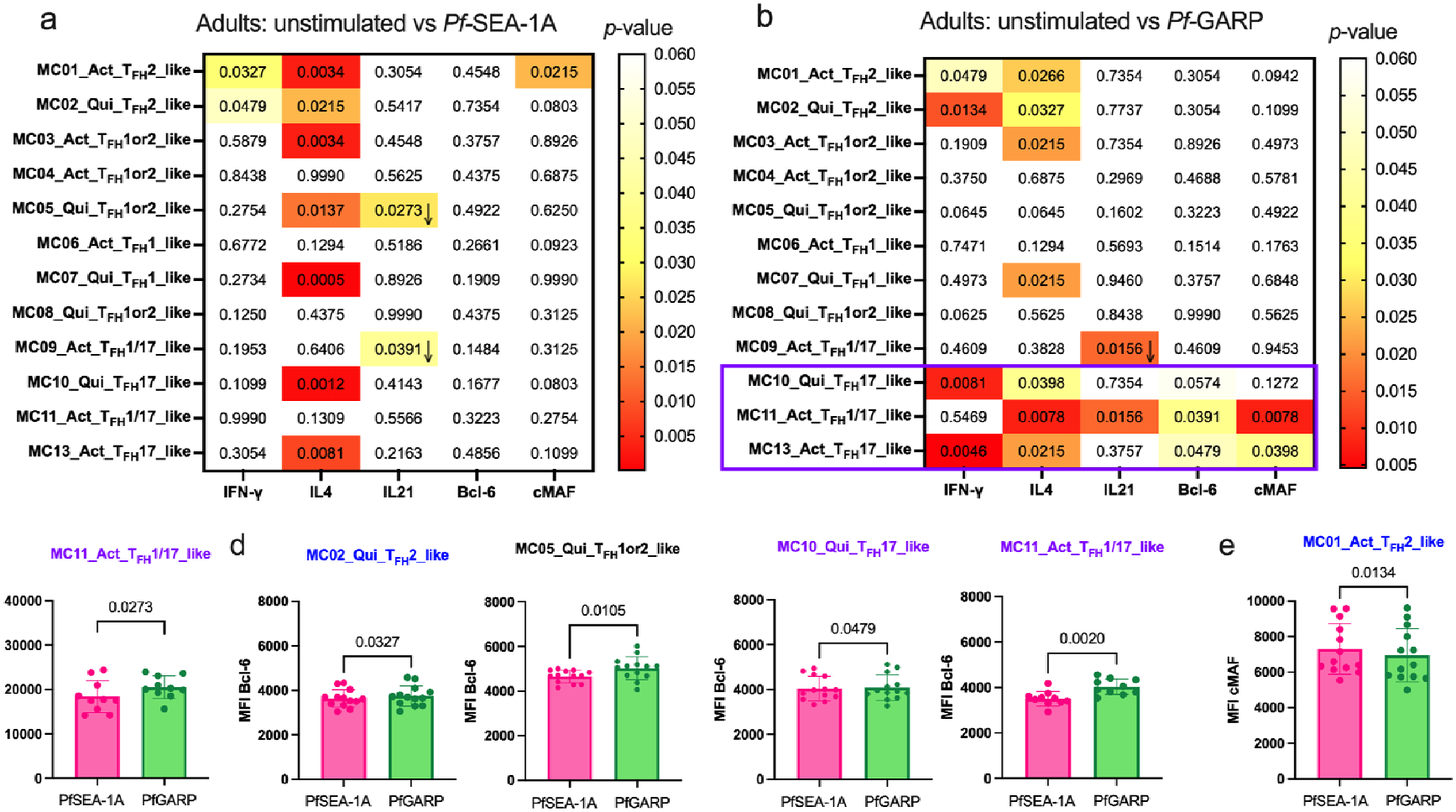
a
Adults: unstimulated vs Pf-SEA-1A
p-value
MC01_Act_TFH2_like 0.0327 0.0034 0.3054 0.4548 0.0215
MC02_Qui_TFH2_like 0.0479 0.0215 0.5417 0.7354 0.0803
MC03_Act_TFH1or2_like 0.5879 0.0034 0.4548 0.3757 0.8926
MC04_Act_TFH1or2_like 0.8438 0.9990 0.5625 0.4375 0.6875
MC05_Qui_TFH1or2_like 0.2754 0.0137 0.0273 0.4922 0.6250
MC06_Act_TFH1_like 0.6772 0.1294 0.5186 0.2661 0.0923
MC07_Qui_TFH1_like 0.2734 0.0005 0.8926 0.1909 0.9990
MC08_Qui_TFH1or2_like 0.1250 0.4375 0.9990 0.4375 0.3125
MC09_Act_TFH1/17_like 0.1953 0.6406 0.0391 0.1484 0.3125
MC10_Qui_TFH17_like 0.1099 0.0012 0.4143 0.1677 0.0803
MC11_Act_TFH1/17_like 0.9990 0.1309 0.5566 0.3223 0.2754
MC13_Act_TFH17_like 0.3054 0.0081 0.2163 0.4856 0.1099
IFN-γ IL4 IL21 Bcl-6 cMAF
0.060 0.055 0.050 0.045 0.040 0.035 0.030 0.025 0.020 0.015 0.010 0.005
b
Adults: unstimulated vs Pf-GARP
p-value
MC01_Act_TFH2_like 0.0479 0.0266 0.7354 0.3054 0.0942
MC02_Qui_TFH2_like 0.0134 0.0327 0.7737 0.3054 0.1099
MC03_Act_TFH1or2_like 0.1909 0.0215 0.7354 0.8926 0.4973
MC04_Act_TFH1or2_like 0.3750 0.6875 0.2969 0.4688 0.5781
MC05_Qui_TFH1or2_like 0.0645 0.0645 0.1602 0.3223 0.4922
MC06_Act_TFH1_like 0.7471 0.1294 0.5693 0.1514 0.1763
MC07_Qui_TFH1_like 0.4973 0.0215 0.9460 0.3757 0.6848
MC08_Qui_TFH1or2_like 0.0625 0.5625 0.8438 0.9990 0.5625
MC09_Act_TFH1/17_like 0.4609 0.3828 0.0156 0.4609 0.9453
MC10_Qui_TFH17_like 0.0081 0.0398 0.7354 0.0574 0.1272
MC11_Act_TFH1/17_like 0.5469 0.0078 0.0156 0.0391 0.0078
MC13_Act_TFH17_like 0.0046 0.0215 0.3757 0.0479 0.0398
IFN-γ IL4 IL21 Bcl-6 cMAF
0.060 0.055 0.050 0.045 0.040 0.035 0.030 0.025 0.020 0.015 0.010 0.005
c
MC11_Act_TFH1/17_like
MFI IL21
0.0273
PfSEA-1A PfGARP
d
MC02_Qui_TFH2_like
MFI Bcl-6
0.0327
PfSEA-1A PfGARP
MC05_Qui_TFH1or2_like
MFI Bcl-6
0.0105
PfSEA-1A PfGARP
MC10_Qui_TFH17_like
MFI Bcl-6
0.0479
PfSEA-1A PfGARP
MC11_Act_TFH1/17_like
MFI Bcl-6
0.0020
PfSEA-1A PfGARP
e
MC01_Act_TFH2_like
MFI cMAF
0.0134
PfSEA-1A PfGARP

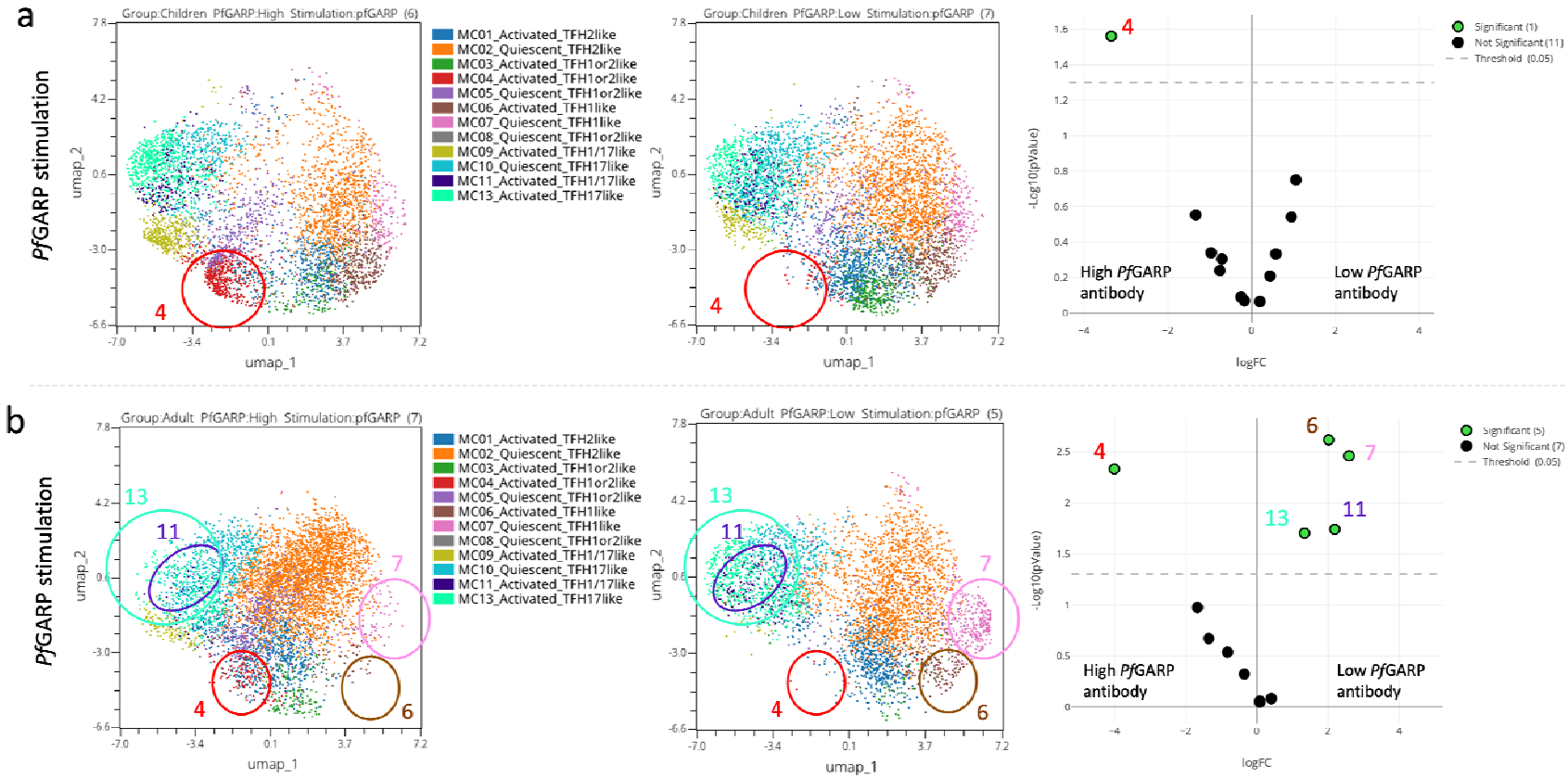
a
PfGARP stimulation
Group:Children PfGARP:High Stimulation:pfGARP (6)
Group:Children PfGARP:Low Stimulation:pfGARP (7)
MC01_Activated_TFH2like
MC02_Quiescent_TFH2like
MC03_Activated_TFH1or2like
MC04_Activated_TFH1or2like
MC05_Quiescent_TFH1or2like
MC06_Activated_TFH1like
MC07_Quiescent_TFH1like
MC08_Quiescent_TFH1or2like
MC09_Activated_TFH1/17like
MC10_Quiescent_TFH17like
MC11_Activated_TFH1/17like
MC13_Activated_TFH17like
umap_1
umap_2
4
Significant (1)
Not Significant (11)
Threshold (0.05)
-Log10(pValue)
logFC
High PfGARP antibody
Low PfGARP antibody
b
PfGARP stimulation
Group:Adult PfGARP:High Stimulation:pfGARP (7)
Group:Adult PfGARP:Low Stimulation:pfGARP (5)
13
11
7
4
6
Significant (5)
Not Significant (7)
Threshold (0.05)

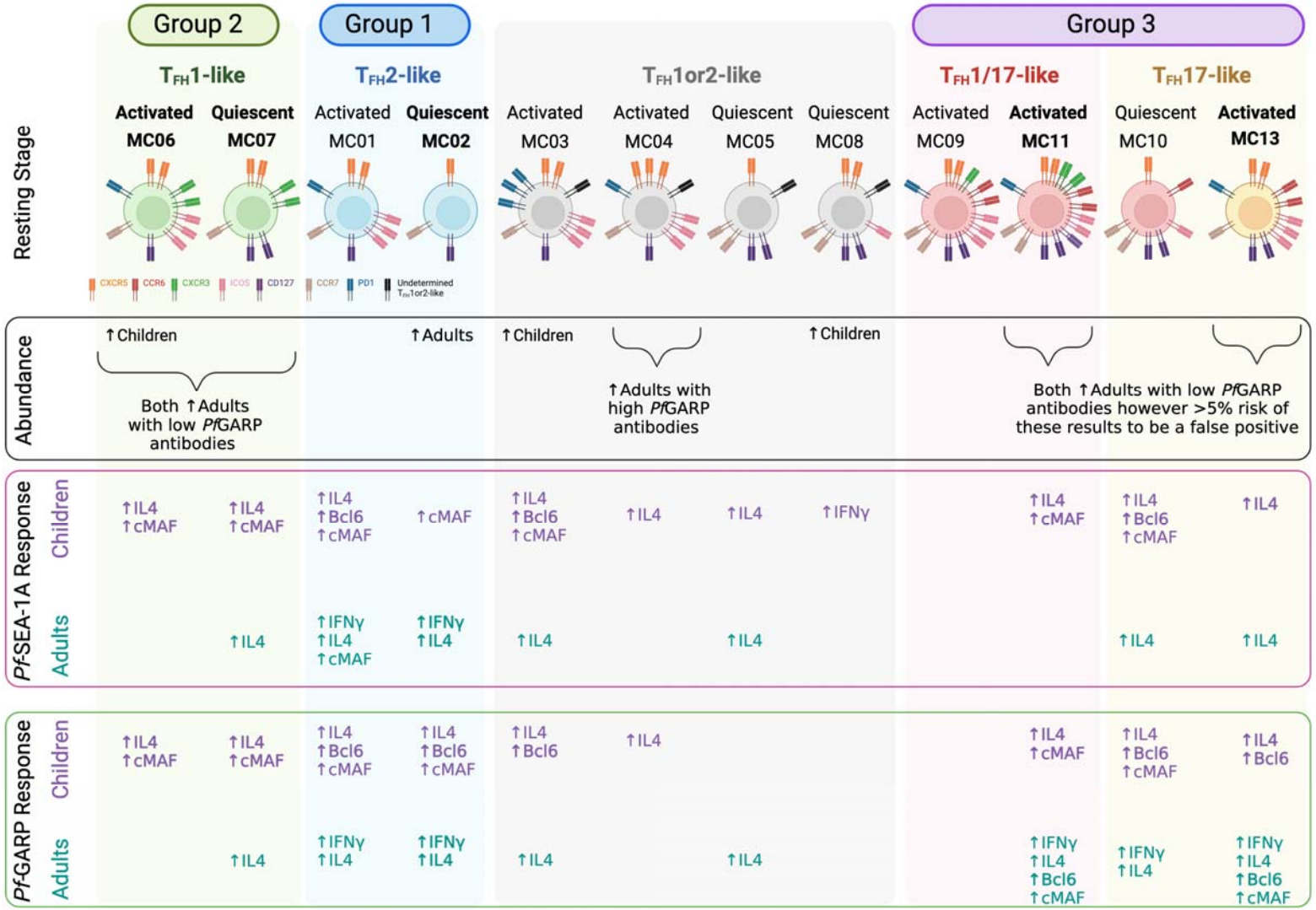
Group 2
Group 1
Group 3
TFH1-like
TFH2-like
TFH1or2-like
TFH1/17-like
TFH17-like
Activated MC06
Quiescent MC07
Activated MC01
Quiescent MC02
Activated MC03
Activated MC04
Quiescent MC05
Quiescent MC08
Activated MC09
Activated MC11
Quiescent MC10
Activated MC13
Resting Stage
CXCR5 CCR6 CXCR3 ICOS CD127
CCR7 PD1 Undetermined TFH1or2-like
Abundance
↑Children
↑Adults
↑Children
↑Children
Both ↑Adults with low PfGARP antibodies
↑Adults with high PfGARP antibodies
Both ↑Adults with low PfGARP antibodies however >5% risk of these results to be a false positive
Pf-SEA-1A Response
Children
↑IL4 ↑cMAF
↑IL4 ↑cMAF
↑IL4 ↑Bcl6 ↑cMAF
↑cMAF
↑IL4 ↑Bcl6 ↑cMAF
↑IL4
↑IL4
↑IFNγ
↑IL4 ↑cMAF
↑IL4 ↑Bcl6 ↑cMAF
↑IL4
Adults
↑IL4
↑IFNγ ↑IL4 ↑cMAF
↑IFNγ ↑IL4
↑IL4
↑IL4
↑IL4
↑IL4
Pf-GARP Response
Children
↑IL4 ↑cMAF
↑IL4 ↑cMAF
↑IL4 ↑Bcl6 ↑cMAF
↑IL4 ↑Bcl6 ↑cMAF
↑IL4 ↑Bcl6
↑IL4
↑IL4 ↑cMAF
↑IL4 ↑Bcl6 ↑cMAF
↑IL4 ↑Bcl6
Adults
↑IL4
↑IFNγ ↑IL4
↑IFNγ ↑IL4
↑IL4
↑IL4
↑IFNγ ↑IL4 ↑Bcl6 ↑cMAF
↑IFNγ ↑IL4
↑IFNγ ↑IL4 ↑Bcl6 ↑cMAF